ELSEVIER

Contents lists available at ScienceDirect

# **Energy & Buildings**

journal homepage: www.elsevier.com/locate/enb



# Thermal optimization of a novel thermo-optically responsive SS-PCM coatings for building enclosures



Zhiying Xiao <sup>a</sup>, Pramod Mishra <sup>b</sup>, Alireza Mahdavi Nejad <sup>c</sup>, Mingjiang Tao <sup>a,\*</sup>, Sergio Granados-Focil <sup>b</sup>, Steven Van Dessel <sup>d,\*</sup>

- <sup>a</sup> Department of Civil and Environmental Engineering, Worcester Polytechnic Institute, 100 Institute Rd, Worcester, MA 01609, USA
- <sup>b</sup> Department of Chemistry, Clark University, 950 Main St, Worcester, MA 01610, USA
- <sup>c</sup>School of Engineering, Wentworth Institute of Technology, Boston, MA 02115, USA
- d Architectural Engineering Program, Department of Civil and Environmental Engineering, Worcester Polytechnic Institute, 100 Institute Rd, Worcester, MA 01610, USA

#### ARTICLE INFO

#### Article history: Received 5 February 2021 Revised 23 April 2021 Accepted 21 May 2021 Available online 24 May 2021

Keywords: Zero energy buildings Phase change materials Transparency shift Numerical simulation

#### ABSTRACT

Building energy consumption constitutes approximately 40% of total energy usage in the US. zero energy buildings (ZEBs) have received much attention in the last decade as they can alleviate some of the negative impacts that buildings have on the environment. New materials and systems are emerging that can help regulate building enclosure heat losses and gains in a passive manner, possibly leading to more cost effective ZEBs. A novel thermo-optically responsive solid-solid phase change material (SS-PCM) coating has been developed to help offset heat gains or losses in building enclosures. The study investigates the optical and thermal processes of the SS-PCM, as well as the synergies among different layers within the enclosure system, through a series of numerical simulations. The impacts of the solar incoming angle and phase transition temperature on the absorptivity of the SS-PCM, which have a significant influence on the optical and thermal transfer processes, are explored. The feasibility and benefits of using the SS-PCM system in building enclosures under both warm and cold climates are investigated. Simulation results: (1) confirm the potential of the SS-PCM coatings to reduce undesirable heat exchange through building enclosure in all orientations and identify the roof as the preferred location of installing the SS-PCM system; (2) substantiate the thermal benefits of the system throughout the year and determine the optimal phase transition temperature of the SS-PCM with maximal energy saving; and (3) demonstrate more thermal benefits and energy saving of the SS-PCM coatings in warm climates compared to cold climates, which has been a challenge for most of existing passive solar facades.

© 2021 Elsevier B.V. All rights reserved.

# 1. Introduction

Rising global population, urbanization, and income lead to increasing demand for energy, with the world energy consumption projected to grow by nearly 50% between 2018 and 2050 [1]. Energy consumed in residential and commercial buildings will increase by 65% during the same time period [1]. The building sector also contributes to 39% of process-related global greenhouse gas emission. Therefore, more efficient and sustainable energy technologies, such as those enabling nearly or net-zero energy buildings(NZEBs), are critical for achieving long term sustainability and climate neutrality [2].

For decades, researchers have studied different approaches and technologies to achieve ZEBs, and many different NZEBs are

E-mail addresses: taomj@wpi.edu (M. Tao), svandessel@wpi.edu (S. Van Dessel).

already reported all over the world [3–5]. The ZEB strategies can generally be divided into two categories, (i) minimization of energy consumption in buildings through energy-efficient measures (e.g. insulating materials, insulated windows, advanced heating and cooling systems and modern lighting) [6], and (ii) the use of renewable energy and other technologies to meet the remaining energy needs. The development of passive solar enclosure technologies based on advanced materials is particularly attractive because it can offer cost-effective alternatives. Passive solar enclosures include Trombe walls [7,8], transparent insulation [9–12], double skin façades [13,14], and so forth.

One type of advanced building materials already used in buildings are thermochromic (TC) materials, which are capable of reversibly altering optical properties due to a temperature difference. Such a feature can modulate solar heat gain or loss of the building enclosure by dynamically managing solar energy, i.e., limiting undesired solar heat gain during the hot seasons and allowing

<sup>\*</sup> Corresponding authors.

#### Nomenclature

Absorptivity of the Phase Change Materials Time (s)  $A_{pcm}$ Specific heat capacity (I/kg·K)  $c_p$ d Thickness (m) Greek letter  $E_t, E_{t,b}, E_{t,d}, E_{t,r}$  Total clear-sky irradiance, the beam component, reflectance of exterior surface and back reflector  $\rho_{12}, \rho_{23}$ the diffuse component, the ground-reflected component angle between sun line and surface normal line 3 Surface emissivity convection coefficient (W/m<sup>2</sup>·K) h Absorbing coefficient (m<sup>-1</sup>)  $\kappa$ radiative intensity as a function of thickness, initial I(x),  $I_0$ Extinction coefficient (m<sup>-1</sup>) F radiative intensity (W/m<sup>2</sup>) Transmittance k Thermal conductivity (W/m·K) L Total length of the system (m) Subscriptions Qs specific heat (J/kg·K) Transparent phase t latent heat (J/kg)  $Q_{I}$ Opaque phase Refractive index n Interior int Scattering coefficient (m<sup>-1</sup>) S Exterior ext T Temperature (°C) Temperature that phase starts to change from opaque to  $T_o, T_t$ transparency, temperature that phase starts to change from transparency to opaque (°C)

more solar heat gain during the cold seasons [15]. The applications of TC materials have already been studied in smart windows and smart building coatings [16,17]. There are numerous advantages of using such TC material on buildings, which includes the application as a passive design to maintain visible light transmittance while controlling NIR transmittance [18], convenient manufacture, simple structures [19,20], and are relatively low in cost [21]. However, some limitations in these systems, including low visible transmittance, high transition temperature, and limited solar modulation capability, require additional studies [22].

Another type of advanced building materials used in building enclosures are phase change materials (PCMs), which are often employed in thermal energy storage (TES) systems to buffer diurnal thermal swings [23–28]. The proper implementation of PCMs in buildings can reduce the peak heating and cooling loads, thus minimizing size and energy consumption of the corresponding thermo-regulating devices. The most used materials for TESs are solid-liquid PCMs (SL-PCMs), which include paraffins, salt hydrates, and various mixtures. However, inherent drawbacks of SL-PCMs limit their more widespread implementation, such as the need for encapsulation to avoid leakage when in liquid state, low thermal conductivity, and thermal hysteresis [29,30]. More recently, solid-solid PCM (SS-PCMs) have been evaluated as potential alternative TESs [31]. SS-PCMs circumvent the need for encapsulation since they retain their shape within the application temperature ranges. SS-PCMs also exhibit less phase separation, degradation, and thermal hysteresis during thermal cycling.

In principle, an advanced material capable of modulating solar heat absorption by two mechanisms, thermo-responsive optical properties and heat storage via reversible phase transitions, is highly desirable for enhancing building energy efficiency and helping achieve ZEBs. A novel thermo-optically responsive SS-PCM polymeric material has been synthesized by our group which has a polymethacrylate backbone containing alkyl pendant phase changing motifs [32,33]. The polymer is opaque in its crystalline form and becomes transparent in the amorphous phase upon heating. This temperature-dependent transparency enables the material to passively control the admittance of the solar energy, while the SS-PCM latent heat provides a high heat storage capacity. Fig. 1 illustrates the change of transparency of the SS-PCM after the phase transition.

Combined with a back-reflector, a novel thermo-optically responsive SS-PCM coating (see Fig. 2) can be integrated into the

building envelope to help reduce energy consumption used for heating and cooling. This study builds upon a recent exploratory study, in which a one-dimensional numerical simulation was carried out on such an SS-PCM based system on building enclosures in a typical central Massachusetts climate [32]. Previous results have shown that such a system can have a positive impact on building thermal performance and can lead to significant energy savings.

The feasibility of incorporating such an SS-PCM based thermoregulating coatings into the building envelop to improve its energy efficiency has been confirmed from the previous study [32]. However, the understanding of the underlying optical and thermal transport processes within the SS-PCM, as well as the synergies or interactions between different layers comprised in the enclosure system, remains limited. The SS-PCM previously proposed had not yet been optimized for achieving maximum energy savings, and it has proven challenging to develop a system that works for both heating- and cooling-dominant climates [2], thus further investigation of the coating's performance under different climate conditions is necessary. This work aims to fill this knowledge gap by examining: (1) impacts of solar incoming angle on the thermal performance of the SS-PCM based coatings on building enclosure in all orientations through sing-day simulations; (2) the overall benefits of the SS-PCM based coatings on building enclosure throughout a year-long duration and the impacts of phase transition temperature on the thermal performance of the SS-PCM based coatings; and (3) the thermal benefits of the system on building enclosure under heating- and cooling-dominant climates.

The next section describes the synthesis & characterization of the SS-PCM coatings and conceptual principles of the system. The modeling methodology and the optimization strategies for determining optical parameters of the SS-PCM are also detailed in Section 3. Section 4 presents and discusses the results of the simulations. The main conclusions from this study are provided in Section 5.

#### 2. Methodology

### 2.1. Polymer synthesis

The novel SS-PCM coatings were synthesized by thermally crosslinking a copolymer containing Stearyl Acrylate (PSA),





Fig. 1. the change of transparency in two phases. Left: cold, crystalline, and opaque. Right: hot, amorphous, transparent.

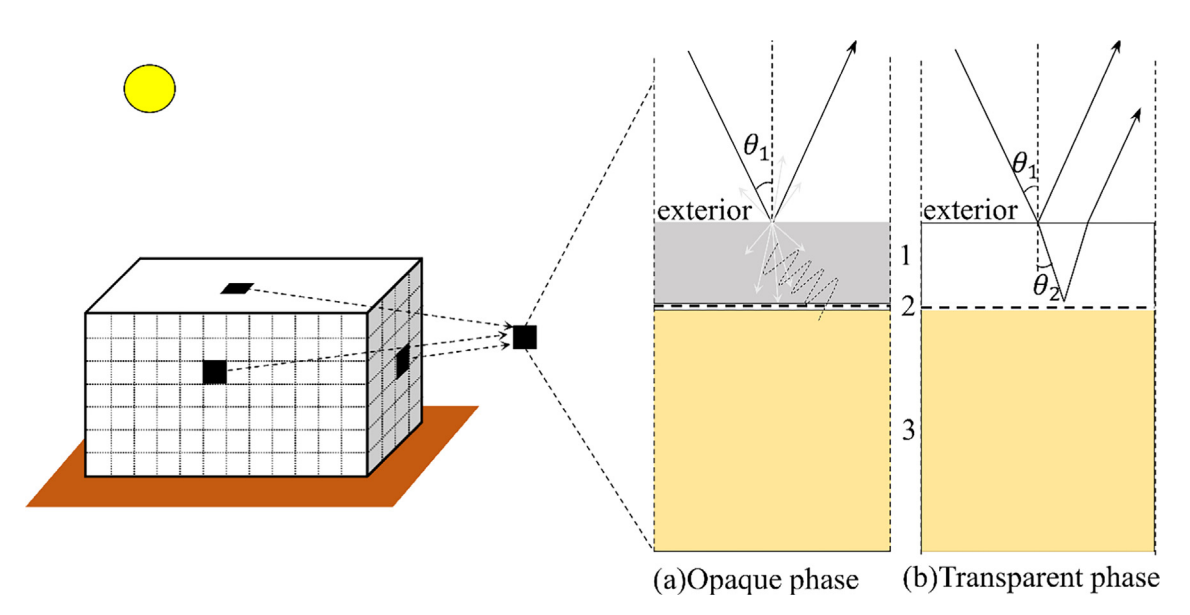


Fig. 2. sketches of the operational principle of the coating system. (a) Opaque phase. The SS-PCM is cold and crystal. (b) Transparent phase. The SS-PCM is warm and amorphous. 1, 2 and 3 stands for 1-mm SS-PCM, a back reflector and a 75-mm insulator, respectively.

Glycidyl Methacrylate (PGMA) and Hexyl Acrylate (HA) in the polymer backbone. The synthesis of these macromolecules was carried out as described in our previous work [33]. The properties of the SS-PCM coating system used for this study are listed in Table 1.

# 2.2. Characterization of SS-PCMs

A glass coated with 1 mm SS-PCM film was used to characterize optical properties in the UV-Vis and Near Infra-Red region of the electromagnetic spectrum. A PerkinElmer Lambda 35 UV/Vis Spectrometer was used to acquire transmittance and reflectance data in

**Table 1** Physical and thermal properties of the system.

| Thermal properties | d [m]              | k [W/m⋅K]        | $Q_s$ [kJ/kg·K]  | $Q_L$ [kJ/kg]   | Density kg/m³    | n                | 3             | reflectance            |
|--------------------|--------------------|------------------|------------------|-----------------|------------------|------------------|---------------|------------------------|
| SS-PCM             | 0.001 <sup>a</sup> | 0.3 <sup>a</sup> | 2.3 <sup>a</sup> | 70 <sup>a</sup> | 930 <sup>a</sup> | 1.5 <sup>b</sup> | 0.9°          | $\rho_{12}(\theta)$    |
| Back reflector     | -                  | _                | -                | -               | _                | -                | -             | $\rho_{23} = 0.95^{c}$ |
| Insulator          | 0.075 <sup>b</sup> | $0.2^{b}$        | 1.5 <sup>b</sup> | _               | 400 <sup>b</sup> | -                | $0.9^{\rm b}$ | -                      |

a: values were obtained by measurement.

b: values were assigned an average value based on similar materials.

c: values were chosen from literature [32].

UV–Visible region (wavelength = 1000 - 300 nm). A scan rate of 480 nm/min with a data interval of 1 nm was used to acquire all UV–Vis spectra. Based on the measured transmittance and reflectance data, the absorption spectrum,  $A_{pcm}(\lambda)$ , of the SS-PCM coating in both phases is presented in Fig. 3.

The enthalpy of melting and the crystalline-to-amorphous transition temperature of the SS-PCMs were determined using a 7 Perkin Elmer Differential Scanning Calorimeter (DSC). Ice-water was used as a cooling system while a continuous flow of nitrogen at 20 ml/min was used to maintain inert environment at the sample and reference furnace. A Heating rate of 10 °C/min and temperature range of 5 °C -90 °C were used to characterize sample weighing approximately 15 mg.

## 2.3. Conceptual system

The SS-PCM based coating system is placed on the exterior of a building enclosure, as schematically shown in Fig. 2. This system has been designed to reduce undesirable heat exchange as follows (see Fig. 2): (1) At low temperature, the SS-PCM is crystalline and remains opaque to solar radiation; thus, the optical absorptivity of solar irradiance can be tuned to allow for more energy gains during cold seasons as a dark surface does; and (2) When heated above its phase transition temperature, the SS-PCM becomes amorphous and transparent after undergoing a reversible phase change. Most of the solar irradiance transmits through the SS-PCM onto a back reflector and then reflects back to the environment as a light surface does. Therefore, minimal solar radiation will be absorbed by the system and the overall thermal performance is better compared to that of both the dark and light surface.

#### 2.4. Governing equations

Fig. 5 illustrates the 1-d model geometry and material properties of the system. The Finite element models were implemented in COMSOL (Multiphysics 5.4) using linear elements with a constant length of 0.5 mm for the model.

Assumptions for the mathematical model are listed below:

(1) The heat transfer through the system is simplified to a onedimensional unsteady heat transfer process.

- (2) The contact thermal resistance of the interfaces within the system is omitted.
- (3) The SS-PCMs are thermally homogeneous and isotropic media, and the thermal conductivities of the materials are temperature independent.
- (4) The specular reflection of the back reflector is assumed to be a constant.

The heat transfer process of the SS-PCM coating is illustrated in Fig. 4. The energy equation is given by the heat equation (1a) [34]:

$$\rho_{pcm}c_p(T)\frac{\partial T}{\partial t} = \frac{\partial}{\partial x}\left(k_{pcm}\frac{\partial T}{\partial x}\right) + \dot{q}_r(x,t) \tag{1a}$$

$$c_p(T) = \frac{dH}{dT} \tag{1b}$$

$$H = Q_s \hat{A} \cdot T + step \hat{A} \cdot Q_L \tag{1c}$$

$$step = \begin{cases} 0, T < T_o \\ \frac{T - T_o}{T_t - T_o} \\ 1, T > T_t \end{cases}, T_o \le T \le T_t$$
 (1d)

Where: t is time (s). $\rho_{pcm}$  is the density (kg/m³).  $c_p(T)$  is the specific heat capacity (J/kg·K).  $k_{pcm}$  is the thermal conductivity (W/m·K).  $\dot{q}_r$  is the heat source from solar radiation (W/m²). H is the enthalpy (J/kg). H0. H1 are the specific heat (J/kg·K) and latent heat (J/kg) of the SS-PCM respectively.

The governing equation for the insulator is given as:

$$\rho_{in}c_{p,in}\frac{\partial T}{\partial t} = \frac{\partial}{\partial x}\left(k_{in}\frac{\partial T}{\partial x}\right) \tag{1e}$$

Where  $\rho_{in}$   $c_{p,in}$  and  $k_{in}$  are density (kg/m³), specific heat capacity (J/kg·K) and thermal conductivity (W/m·K) of insulator, respectively.

#### 2.4.1. The heat source term $\dot{q}_r(x,t)$

 $\dot{q}_r(x,t)$  is the quantity of solar energy absorbed by the SS-PCM coating, which can be determined by the total incoming irradiation  $(E_t)$  and the absorptivity  $(A_{pcm})$  of the material. The property which distinguishes this SS-PCM from traditional PCMs is the change of absorptivity when it undergoes the phase transition from opaque

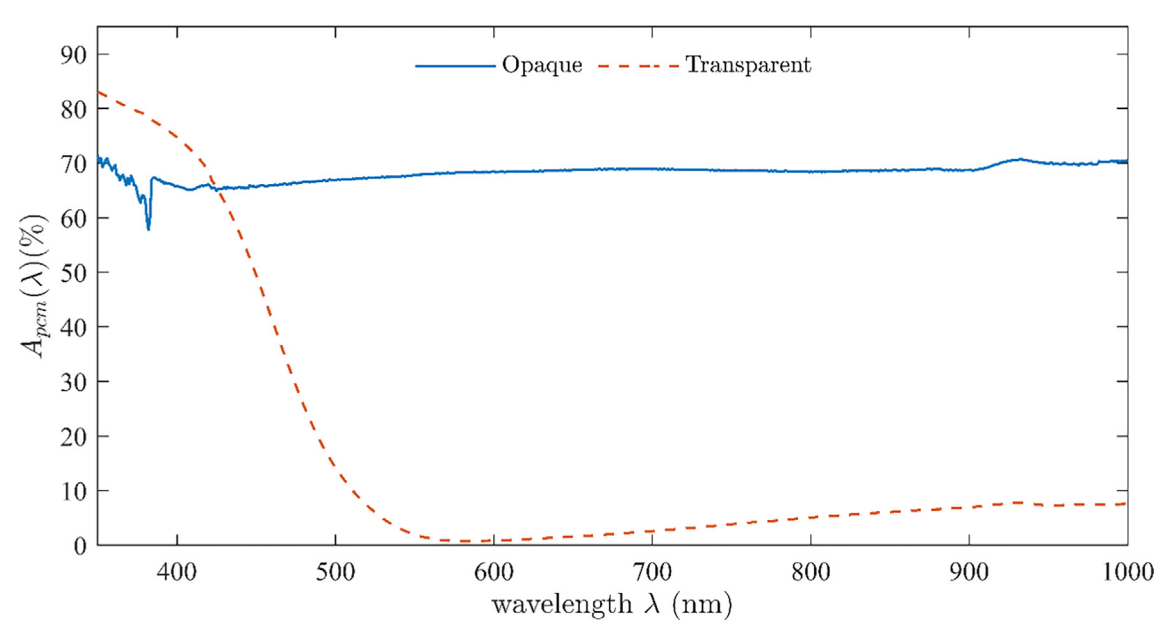


Fig. 3. spectrum absorptivity of the SS-PCM coating in opaque phase and transparent phase.

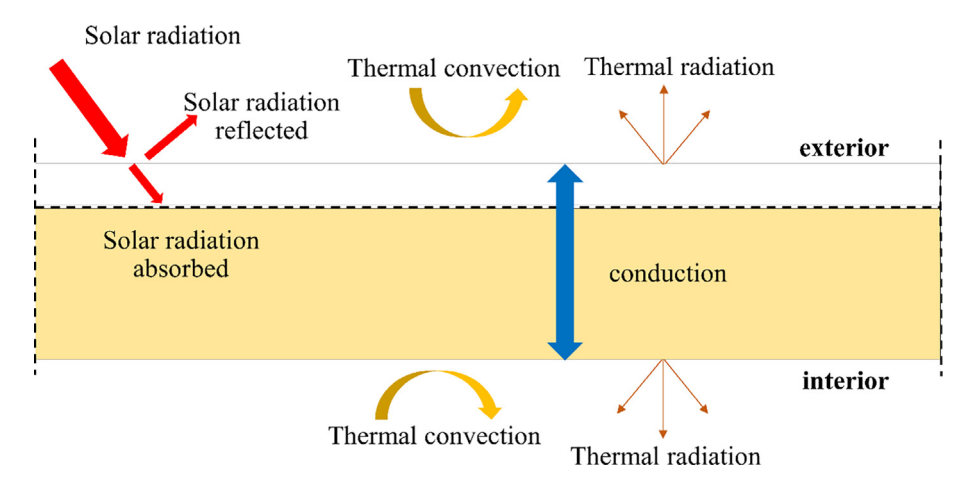
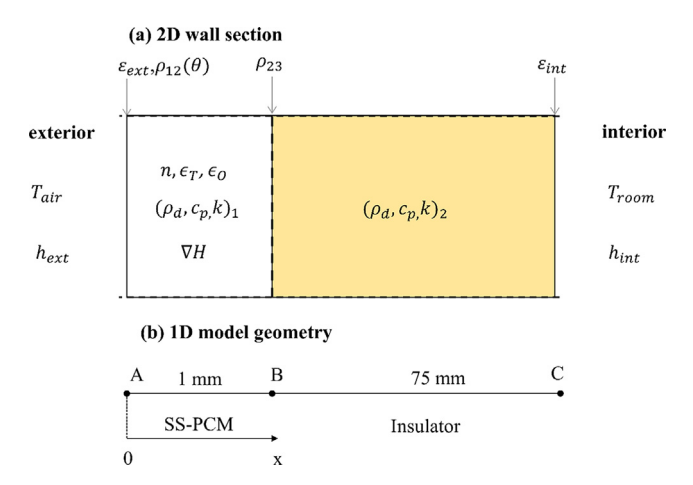


Fig. 4. heat transfer processes of the SS-PCM based coating system.



**Fig. 5.** (a): A schematic of the material properties and system parameters, (b): A schematic of the 1D model.

state to transparent state.  $\dot{q}_r$  is zero for the insulator layer since radiation transferred into the insulator is negligible. The total incoming irradiation  $(E_t)$  and the absorptivity  $(A_{pcm})$  should be first obtained in order to determine  $\dot{q}_r(x,t)$ , which are presented by a step-by-step procedure in the following paragraphs.

Total solar radiation ( $E_t$ ) can be calculated using equations (2) from ASHRAE [35].

$$E_t = E_{t,b} + E_{t,d} + E_{t,r} (2)$$

Total clear-sky irradiance  $(E_t)$  reaching the receiving surface is the sum of three components: the beam component  $(E_{t,b})$  originating from the solar disc; the diffuse component  $(E_{t,d})$  originating from the sky dome; and the ground-reflected component  $(E_{t,r})$  originating from the ground in front of the receiving surface. In the equations from ASHRAE, solar irradiance varies with angles between surface normal line and solar-earth line, and solar irradiance also changes from season to season. Thus, it is necessary to simulate the heat transfer process on walls of different orientations and implement year-long simulations in order to capture a comprehensive understanding of benefits of the SS-PCM coating on building enclosures.

Absorptivity  $A_{pcm}$ , is an important optical property that indicates the ratio of radiative energy absorbed by an optical medium to the total energy reaching the medium. Absorptivity of the SS-PCM undergoes a significant change during the phase transition, it consequently affects the heat source term as shown in equation

(1). Therefore, the absorptivity that depends on the SS-PCM's thermal and optical transfer processes is influenced by their synergies. In the transparent phase, the coating allows transmission of most of the radiation through the medium while only part of the radiation is reflected to the ambient from the exterior surface of the SS-PCM. The absorptivity should be determined separately for the transparent phase  $A_{pcm,t}$  and opaque phase  $A_{pcm,o}$ . The absorptivity  $A_{pcm,t}$  of transparent phase was computed by equation (3a), depending on the extinction coefficient,  $\epsilon$ , and the reflectance,  $\rho_{12}$ , of the exterior surface.  $\rho_{12}$ , relies on the refractive index and incoming angle and can be obtained by Fresnel's Law [34].

$$A_{pcm,t} = \frac{(1-\rho_{12})(1+\rho_{23}\tau)(1-\tau)}{1-\rho_{12}\rho_{23}\tau^2} \tag{3a}$$

$$\tau = e^{-\epsilon_t \cdot d/\cos\theta_2} \tag{3b}$$

$$\epsilon_t = \kappa_t + \mathsf{s}_t \tag{3c}$$

$$\rho_{12} = \frac{1}{2} \left[ \left( \frac{\cos\theta_2 - n\cos\theta_1}{\cos\theta_2 + n\cos\theta_1} \right)^2 + \left( \frac{\cos\theta_1 - n\cos\theta_2}{\cos\theta_1 + n\cos\theta_2} \right)^2 \right] \tag{3d}$$

Where  $\rho_{12}$  and  $\rho_{23}$  are the reflectance of the exterior surface and the back reflector, respectively;  $\tau$  is the transmittance of SS-PCM;  $\kappa_t, s_t \text{and} \epsilon_t$  are the absorbing coefficient, scattering coefficient and extinction coefficient of the SS-PCM during transparent phase, respectively; n is the refractive index of the SS-PCM. d is the thickness of the coating;  $\theta_1$  and  $\theta_2$  are the incidence angle and reflection angle correspondingly as shown in Fig. 2.

While in the opaque phase, the scattering effect plays an important role since solar radiation would be absorbed and reflected by scattering when interacting with the polymer molecules. Thus, K-M theory [36,37] was adopted to compute the absorptivity,  $A_{pcm,o}$ .

$$A_{\textit{pcm,o}} = \frac{(2\beta_{\textit{km}} + 2\beta_{\textit{km}}^2)e^{\alpha_{\textit{km}}d/\cos\theta_2} + (2\beta_{\textit{km}} - 2\beta_{\textit{km}}^2)e^{-\alpha d/\cos\theta_2} - 4\beta_{\textit{km}}}{[(1+\beta_{\textit{km}})^2e^{\alpha_{\textit{km}}d/\cos\theta_2} - (1-\beta_{\textit{km}})^2e^{-\alpha_{\textit{km}}d/\cos\theta_2}](1+\rho_{12})} \tag{4a}$$

$$\alpha_{km} = \sqrt{\kappa_o(\kappa_o + 2s_o)} \tag{4b}$$

$$\beta_{km} = \sqrt{\frac{\kappa_o}{\kappa_o + 2s_o}} \tag{4c}$$

Where  $\kappa_0$  and  $s_0$  are the absorbing coefficient and scattering coefficient of the SS-PCM during opaque state, respectively.

#### 2.4.2. Boundary and initial conditions

The boundary conditions at x = 0 and x = L of the model are schematically shown in Fig. 5 which are calculated by equation (5a) and (5b):

$$-k_{pcm}\frac{\partial T}{\partial x}|_{x=0} = h_{ext}(T_{air}-T) + \varepsilon_{ext}\sigma(T_{air}^4-T^4) \eqno(5a)$$

$$-k_{in}\frac{\partial T}{\partial x}|_{x=L} = h_{int}(T - T_{room}) + \varepsilon_{int}\sigma(T - T_{room}^4)$$
 (5b)

Where  $h_{ext}$  and  $h_{int}$  are exterior convection coefficient and interior convection coefficient respectively;  $\varepsilon_{ext}$  and  $\varepsilon_{int}$  are exterior and interior surface emissivity, respectively.  $\sigma$  is the Stefan–Boltzmann constant. L is the total thickness of system. The initial temperature is set to 25 °C throughout the model.

The external convective heat transfer,  $h_{ext}$ , is derived using the relationship that factors in the surface-to-wind angle and wind velocity. These correlations have been derived using CFD tools and have been validated using experimental data [38]. The internal convective heat transfer coefficient,  $h_{int}$ , is determined based on a correlation derived from a large experimental test cell [39]. The weather parameters required in the model include the external air temperature,  $T_{air}$ , wind velocity and wind direction. The room temperature,  $T_{room}$ , is set to 25 °C in the study. Other weather parameters used in the simulation are the number of clear-sky days and complete overcast-sky days. Geographic location and orientation of the building enclosure system are also required.

#### 2.5. Absorptivity-related parameters

The absorptivity, $A_{pcm}$  of SS-PCM coating system that has a significant influence on the optical and thermal transfer process, depends on the optical parameters (e.g., absorption coefficient, scattering coefficient), and is affected by the solar incoming angle and phase transition temperature. Although the absorptivity spectrum is obtained, it can only be used to compute total absorptivity when the solar light is normal to the SS-PCM surface. Therefore, it is important to determine the optical parameter values to capture all the absorptivity values versus solar incoming angle. The absorptivity spectrum presented previously can be transformed to the total absorptivity using equation (6) [34]. The absorptivity values chosen for simulations were 0.7 and 0.1 for the opaque and the transparent phases, respectively. These two values were used to determine optical parameters of the SS-PCM.

$$A_{pcm} = \frac{\int A_{pcm}(\lambda) E_{\lambda}(\lambda) d\lambda}{\int E_{\lambda}(\lambda) d\lambda}$$
 (6)

# 2.5.1. Extinction coefficient

The extinction coefficient  $\epsilon$  determines the distance sunlight travels before becoming extinct within the medium by absorption and scattering. Its value equals the sum of  $\kappa$  and s. It can be determined by solving equation 3(a) for the transparent phase. In the opaque phase,  $\epsilon_o$  needs to be high enough to trap more solar energy, while too high  $\epsilon_o$  leads to a reduction of material utilization. Thus, it is important to determine the  $\epsilon_o$  value to accurately capture the optical and thermal transfer processes within the material. However,  $\epsilon_o$  cannot be obtained directly from K-M theory as shown in equation 4(a).

By introducing the measured average transmittance value, Beer's Law was used to estimate  $\epsilon_o$  for the opaque phase. In this study, the thickness of the SS-PCM coating was set to 1 mm, Thus, the  $\epsilon_o$  value was determined to be 4600  $m^{-1}$  according to equations (7a)  $\sim$  (7c) when the SS-PCM is in its opaque phase and  $\epsilon_t = 53~m^{-1}$  when in the transparent phase according to equation (3a).

$$dI = -I \cdot \epsilon dx \tag{7a}$$

$$\frac{I(d)}{I_0} = e^{-\epsilon d} = transmittance \tag{7b}$$

$$\epsilon = -\frac{\ln{(transmittance)}}{d} \tag{7c}$$

#### 2.5.2. Absorption coefficient $\kappa$ and scattering coefficient s

 $\kappa$  and s represent the absorbing effect and scattering effect, respectively, during the process of optical transfer. According to equations (3a)  $\sim$  (4c), the absorptivity depends on both  $\kappa$  and s. The  $\kappa_t$  can be set as the same as  $\epsilon_t$  since the scattering effect is negligible when in the transparent phase, thus, both  $\kappa_t$  and  $\epsilon_t$  can be determined by solving equation (3c). In addition, it is convenient to obtain  $\kappa_o$  and  $s_o$  for the opaque phase by calculating the ratio,  $\gamma$  of these two values. Therefore, the relationship between ratio,  $\gamma$  and  $A_{pcm,o}$  can be built by substituting  $\kappa_o = \epsilon_o \gamma / (1 + \gamma)$  and  $s_o = \epsilon_o / (1 + \gamma)$  into equations (4a)  $\sim$  (4c), from which the ratio  $\gamma$  was found to be 1.085 and  $\kappa_o$  and  $s_o$  were obtained to be 2400  $m^{-1}$  and 2200  $m^{-1}$ , respectively. Henceforth the  $\kappa$  and s were determined for both the opaque and the transparent phases.

# 2.5.3. Solar incoming angle $\theta$

The angle $\theta$  between the solar irradiance and the surface normal line has a significant impact on the solar radiation intensity on the surface and on the optical properties of the SS-PCM coating.  $\theta$  not only affects the solar radiation impinge on the surface according to section 3.4.1, but also influences the absorptivity of the SS-PCM based on equations (3a)  $\sim$  (4c). Since  $\theta$ s are different for walls of different orientations and also vary with time, it is necessary to evaluate the behaviors of the SS-PCM coating systems installed at different locations of a building enclosure. By applying the absorption coefficient and scattering coefficient value from section 3.5.2 and Table 1, the absorptivity curves for both the transparent and opaque phases are obtained and shown in Fig. 6. Fig. 7 shows variations of  $\theta$ s on the hottest day of a year for south, east, west walls and roof separately.

#### 2.5.4. Phase transition temperature

The phase transition temperature is a threshold value, across which phase transition occurs. For the SS-PCM, the phase transition temperature not only controls its phase transition, but it is also a vital parameter directly affecting its transparency, thus influencing the thermal and optical transport processes. An SS-PCM coating with low phase transition temperature is designed to reflect solar irradiant at a relative low temperature, which is favorable in cooling situation but undesirable when more energy gains are needed during cold seasons. Therefore, it is important to investigate the influence of phase transition temperature on the thermal performance of the system and choose a proper phase transition temperature to optimize the overall performance of the SS-PCM based coating system.

The average phase transition temperature, *TT*, is defined as below to simplify the description.

$$TT = \frac{T_o + T_t}{2} \tag{7a}$$

$$T_t - T_o = 10^{\circ} \text{C} \tag{7b}$$

TT should not be very different from building room temperature if it is applied on building enclosure. Usually, the range is around  $20 \sim 30$  °C, and the transition temperature can be tuned by changing the composition of the copolymers during synthesis. The phase

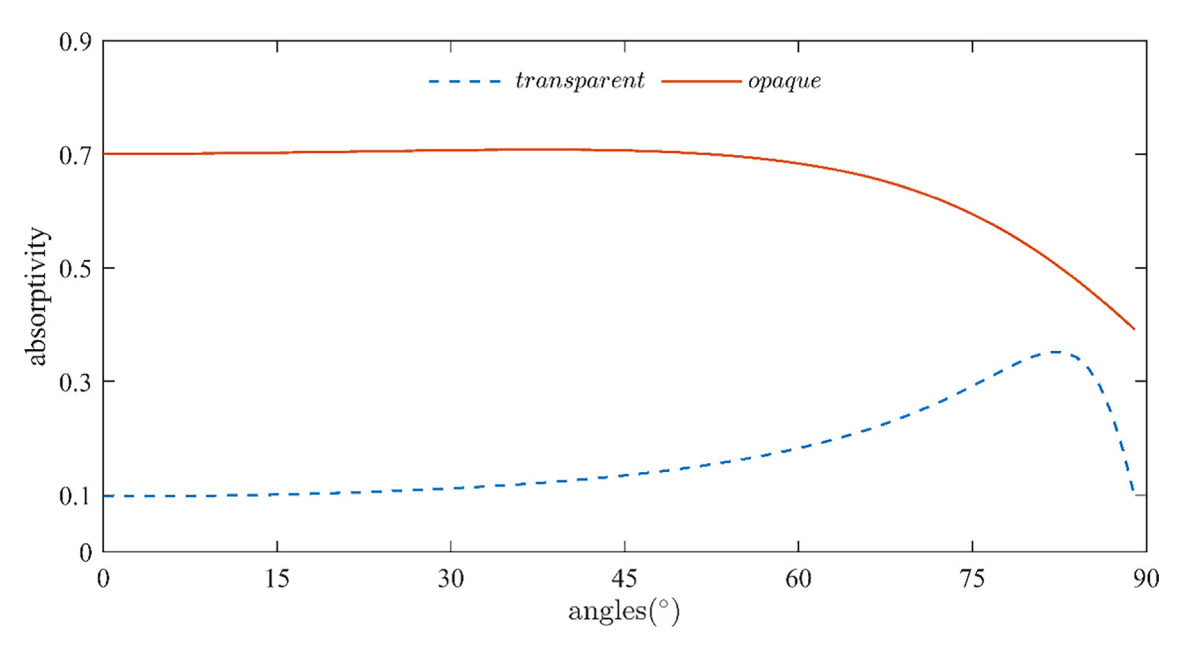


Fig. 6. Absorptivity distribution versus solar incoming angle for both opaque phase and transparent phases.

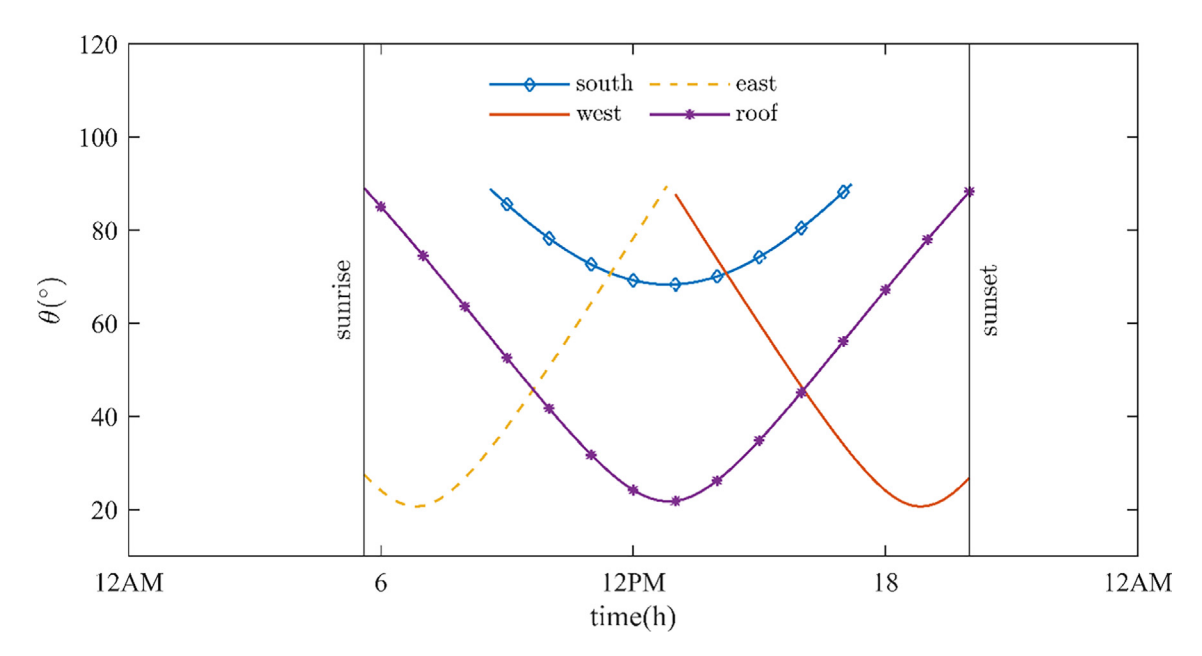


Fig. 7. Incoming angles for different walls in the hottest day.

transition temperature range of the SS-PCM is about 10  $^{\circ}$ C, and the TT mentioned in the paper stands for the mean value of the phase change temperature.

By selecting different transition temperatures, i.e., TT = 20, 25 and 30 °C, it is possible to control the heat exchange of the coating system. Year-long simulations were performed to calculate the energy exchanges to compare the behavior of SS-PCM based coating systems with different TTs.

#### 2.6. Simulation scenarios

Based on the SS-PCM coating-based systems introduced above, Finite Element Method (FEM) models were developed to simulate the heat transfer processes of the proposed building enclosure systems while considering its temperature-dependent transparency

simultaneously. The system properties are summarized in Table 1, and a summary of simulation scenarios is provided in Table 2. The proposed system was assumed to be installed on a building in Boston, Massachusetts. The climate data used in both the single-day and the year-long simulations were extracted from Energy Plus Weather [40]. To verify and quantify the benefits of SS-PCM, a dark color and a light color building enclosure system were chosen as the references, of which the absorptivity were constants of 0.7 and 0.3, respectively.

Scenarios G1-G5 were used to investigate the influence of the enclosure orientations of the SS-PCM system on energy consumption. The performance of the SS-PCM system throughout the year was studied with scenarios G6, while scenarios G6a, G6d and G6e were performed to examine the influence of phase transition temperature of SS-PCM on the thermal behavior of the system.

**Table 2** Simulation scenarios.

| Scenarios | Wall orientations | Material | TT    | Simulation period | absorptivity |
|-----------|-------------------|----------|-------|-------------------|--------------|
| G1-a      | South             | SS-PCM   | 25 °C | Single day        | $A_{pcm}$    |
| G1-b      |                   | dark     | _     | Single day        | 0.7          |
| G1-c      |                   | light    | -     | Single day        | 0.3          |
| G2-a      | East              | SS-PCM   | 25 °C | Single day        | $A_{pcm}$    |
| G2-b      |                   | dark     | -     | Single day        | 0.7          |
| G2-c      |                   | light    | -     | Single day        | 0.3          |
| G3-a      | Roof              | SS-PCM   | 25 °C | Single day        | $A_{pcm}$    |
| G3-b      |                   | dark     | _     | Single day        | 0.7          |
| G3-c      |                   | light    | -     | Single day        | 0.3          |
| G4-a      | West              | SS-PCM   | 25 °C | Single day        | $A_{pcm}$    |
| G4-b      |                   | dark     | _     | Single day        | 0.7          |
| G4-c      |                   | light    | -     | Single day        | 0.3          |
| G5-a      | North             | SS-PCM   | 25 °C | Single day        | $A_{pcm}$    |
| G5-b      |                   | dark     | _     | Single day        | 0.7          |
| G5-c      |                   | light    | -     | Single day        | 0.3          |
| G6-a      | Roof              | SS-PCM   | 25 °C | Year-long         | $A_{pcm}$    |
| G6-b      |                   | dark     | _     | Year-long         | 0.7          |
| G6-c      |                   | light    | =     | Year-long         | 0.3          |
| G6-d      |                   | SS-PCM   | 20 °C | Year-long         | $A_{pcm}$    |
| G6-e      |                   | SS-PCM   | 30 °C | Year-long         | $A_{pcm}$    |

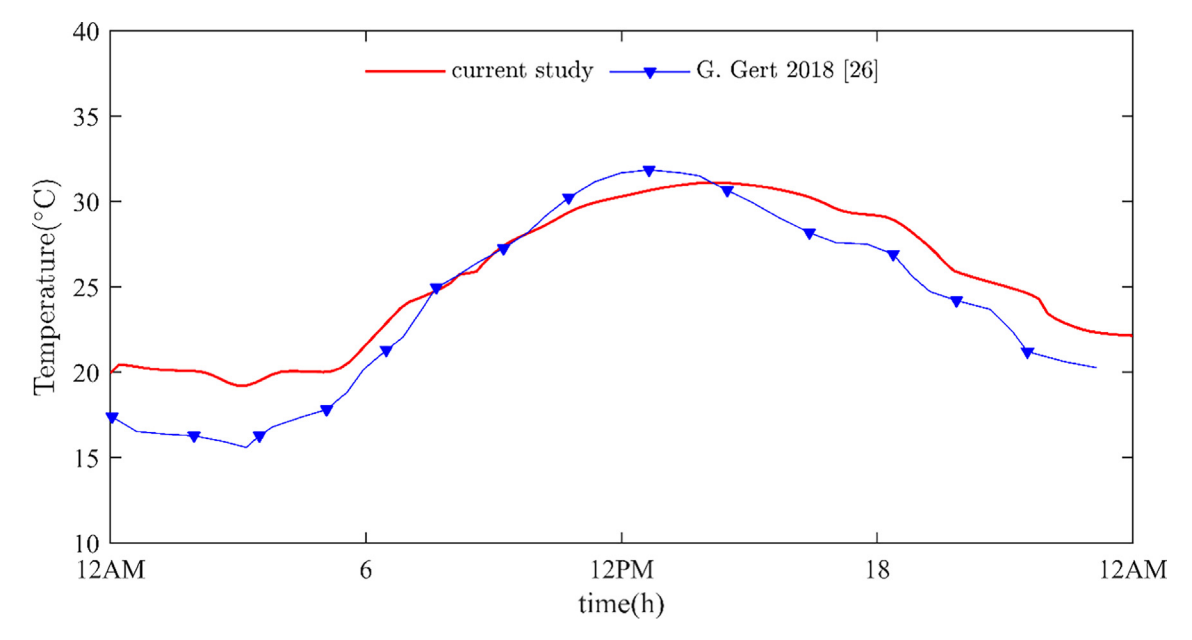


Fig. 8. comparison of temperature of the back reflector of the SS-PCM in this work and the literature [32].

#### 2.7. Model validation

The numerical simulation model was validated by comparing the temperature result of the SS-PCM system with temperature in Fig. 7 from the literature [32]. The system from the literature was evaluated under climate of the warmest day of a typical meteorological year in central Massachusetts and the building enclosure was a south facing vertical wall. The validation model was set as close to the counterpart in the literature as possible, with some slight differences between the two models. The geometry, optical properties and the weather condition for the validation simulations are from Fig. 2 and Table 2 in the literature, while the angle dependency on surface reflectance and the scattering effect are neglected in the reference paper. Fig. 8 shows the comparison of the results between the validation scenario and the data from the reference paper, which shows a good agreement with each

other. However, the peak temperature of the reference paper is higher than that of the current study. One of the reasons is that absorptivity of the SS-PCM in the reference paper is overestimated since the scattering effect is not considered. Some of the parameters such as wind profile were not reported in the literature paper can contribute to the difference of the temperature profiles in Fig. 8.

#### 3. Results and discussion

# 3.1. Influence of orientation of SS-PCM on building envelope

Figs. 9-13 show the results of the SS-PCM coating system applied on walls of different orientations and the roof of the

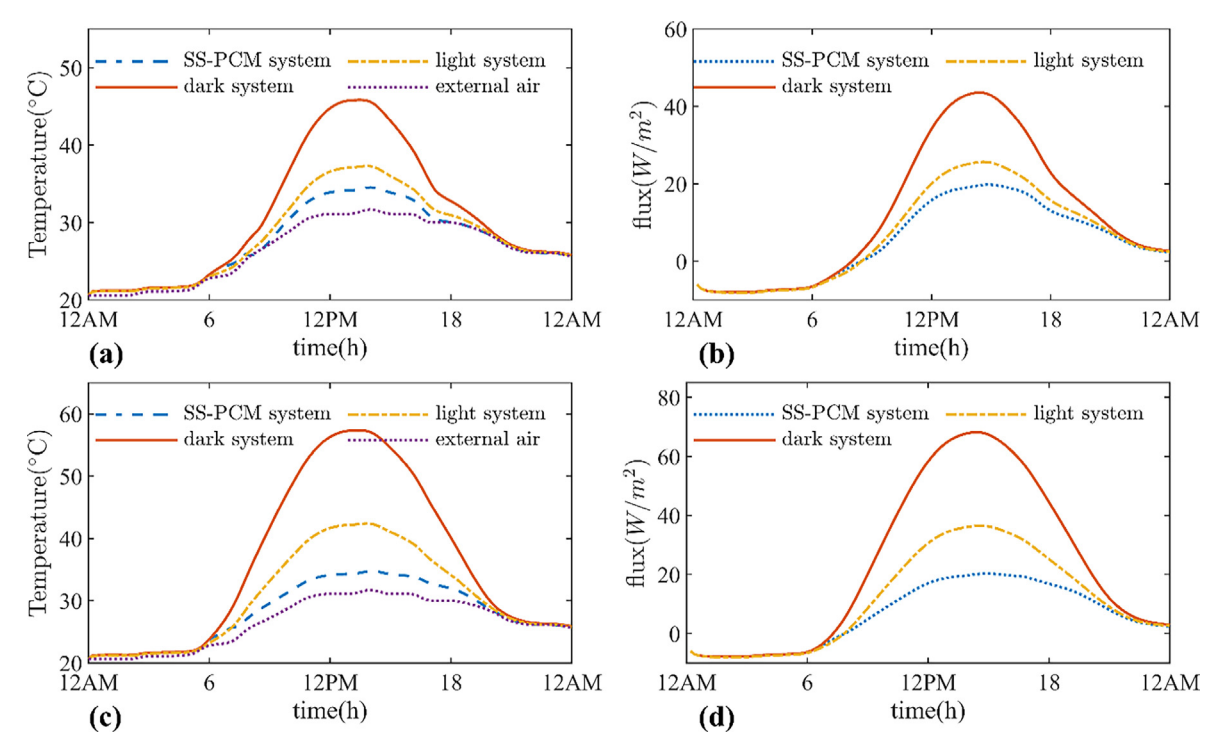


Fig. 9. Diurnal cycle output#1 of back reflector on the hottest day: (a) temperature of the south wall. (b) Flux of the south wall. (c) Temperature of the roof.

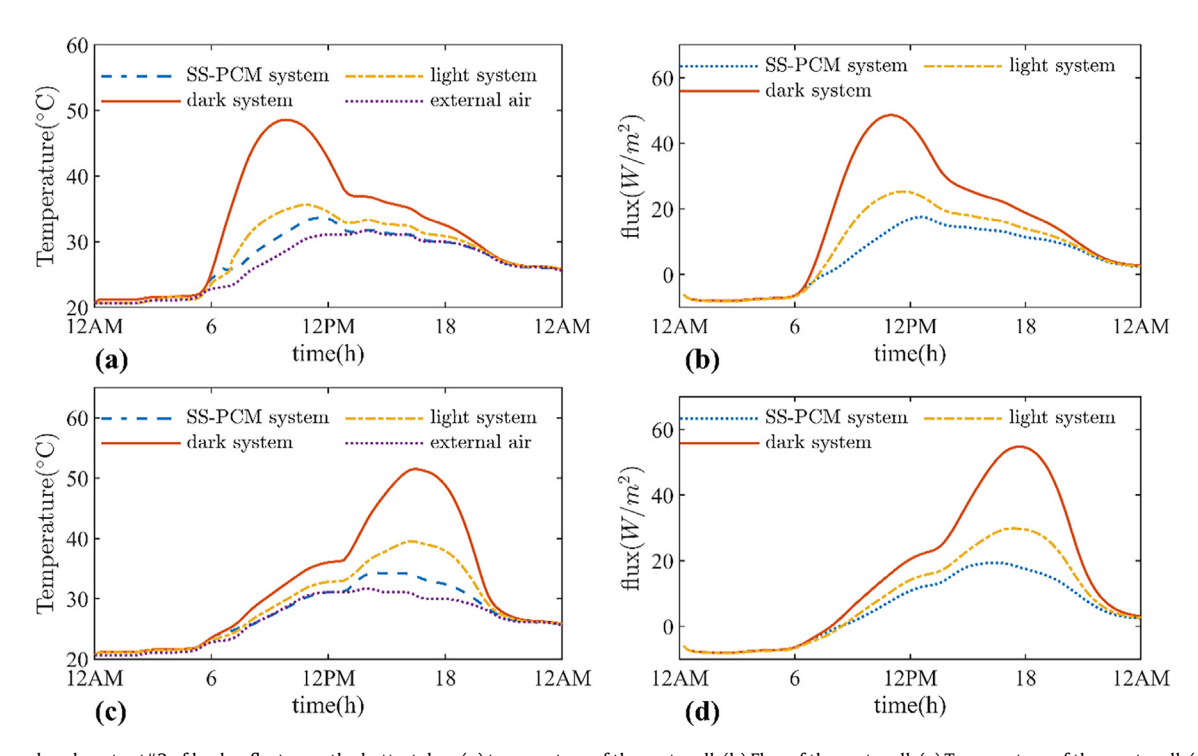


Fig. 10. Diurnal cycle output#2 of back reflector on the hottest day: (a) temperature of the east wall. (b) Flux of the east wall. (c) Temperature of the west wall. (d) Flux of the west wall.

building envelope during a typical 24 h diurnal cycle on the hottest and coldest days in Boston, Massachusetts.

The dark system has the largest temperature and heat flux variation while the SS-PCM system has the smallest, which is desirable, on the hottest day in summer. As shown in Fig. 9(a), the SS-PCM remains opaque from midnight to morning on hot days, since the temperature is around 21 °C, which is below the phase transition

temperature for the south wall. The SS-PCM system and both reference systems exhibit similar temperatures during nighttime on the hottest day since there is no solar radiation during this period. However, different abilities of reflecting, transmitting, and absorbing solar radiation of the systems result in the temperature differences during the daytime. For the south wall, the temperature of the dark system increases dramatically and reaches the highest

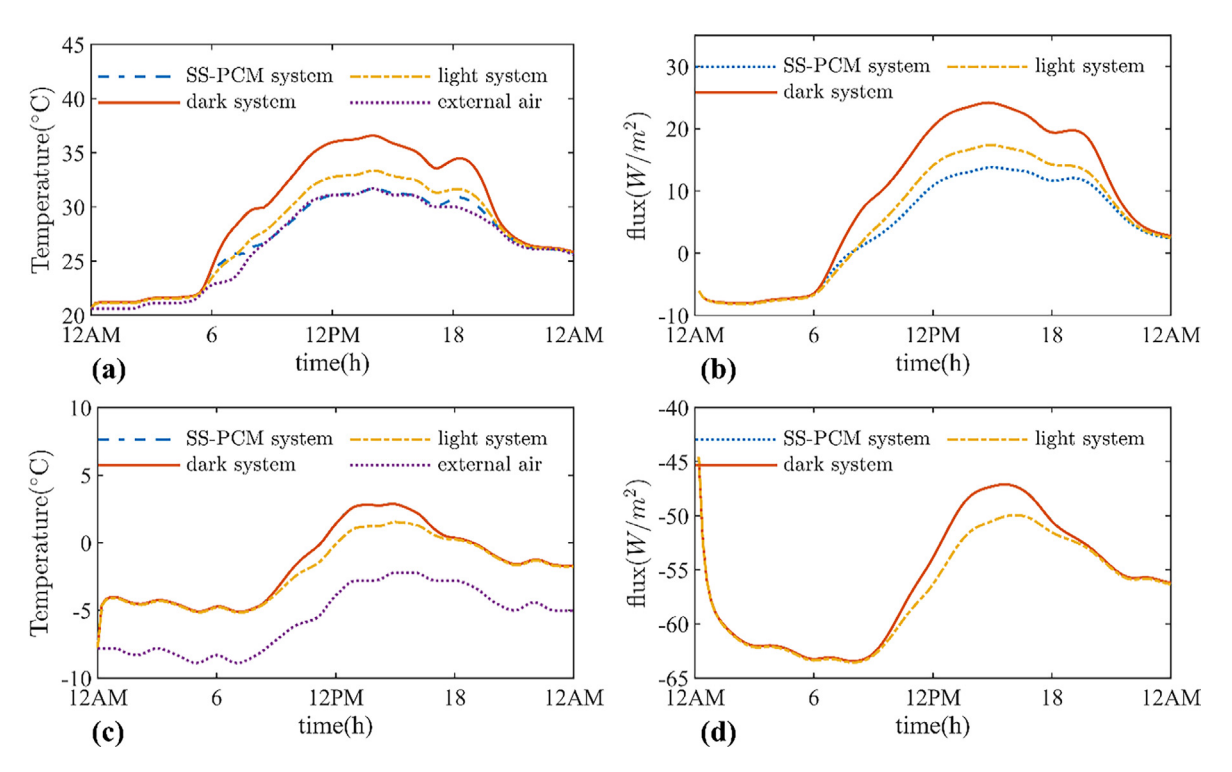


Fig. 11. Diurnal cycle output of back reflector for north wall: (a) temperature on the hottest day. (b) Flux on the hottest day. (c) Temperature on the coldest day. (d) Flux on the coldest day.

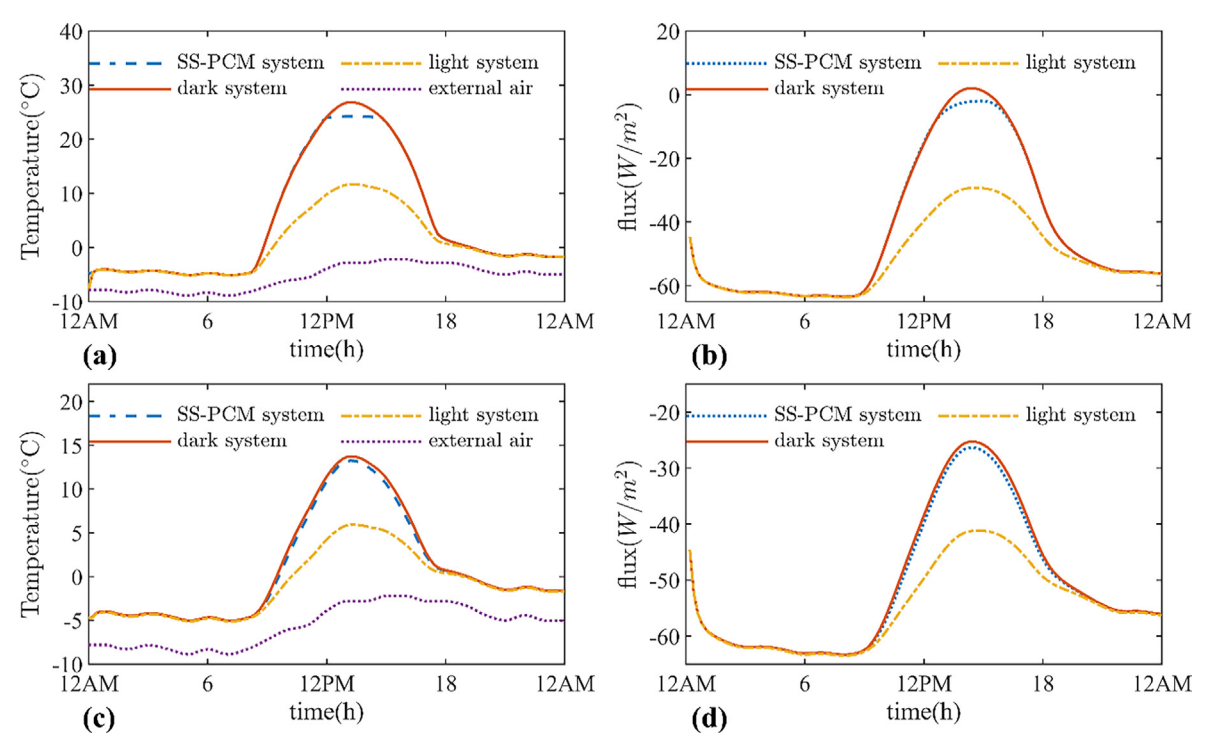


Fig. 12. Diurnal cycle output#1 of back reflector on the coldest day: (a) temperature of the south wall. (b) Flux of the south wall (c) temperature of the roof. (d) Flux of the roof.

value of 45.8 °C at noon, then drops gradually back to the ambient temperature. The light system shows similar pattern to that of the dark system although the highest temperature (37.3 °C) is much lower compared to the maximum for the dark system (45.8 °C). Among the three systems, the SS-PCM shows the least variation

of temperature throughout the simulation time, with the smallest peak temperature of 34.5 °C. Fig. 9(b) shows the heat flux into the room through the interior surface of the south wall. The heat flux profiles indicate that the smallest heat gains (0.124kWh/m²) occur with the SS-PCM coating installed, with larger heat gains (0.296

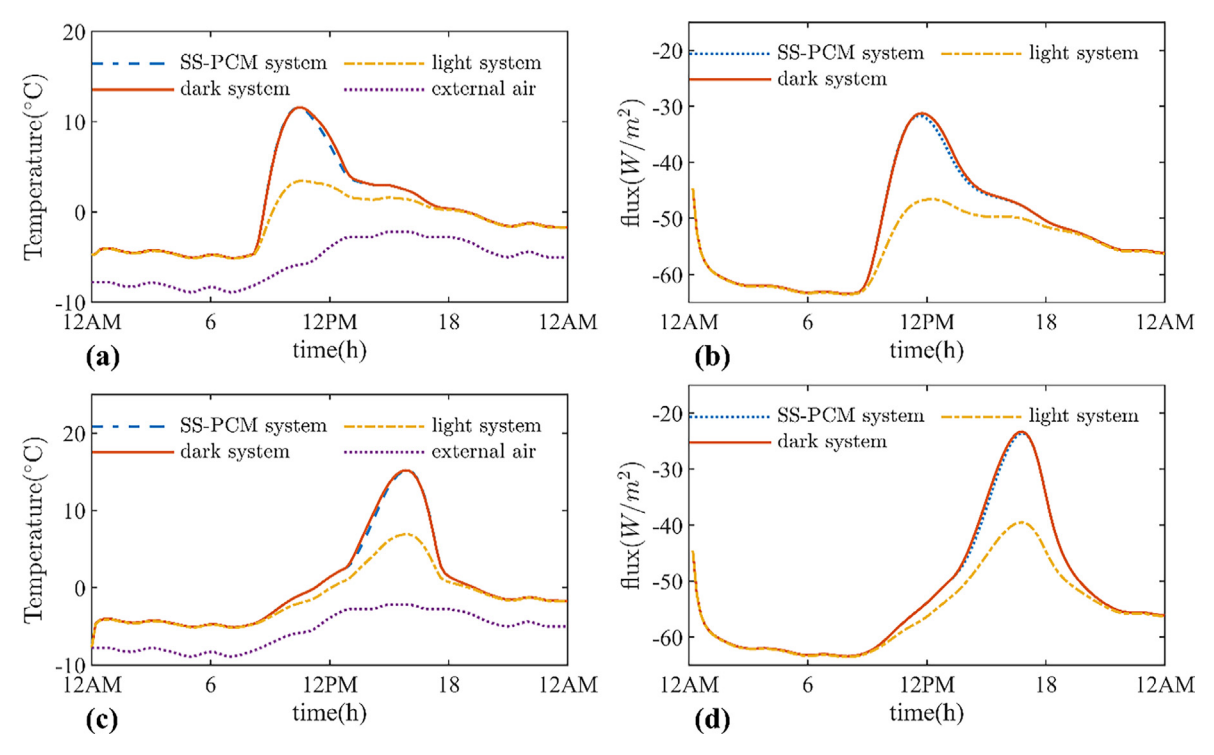


Fig. 13. Diurnal cycle output#2 of back reflector on the coldest day: (a) temperature of the east wall. (b) Flux of the east wall (c) temperature of the west wall. (d) Flux of the west wall.

and 0.164 kWh/m²) occurring in the building with dark and light systems respectively. The temperature and heat flux profiles at other wall orientations of the building enclosures on the hottest day show similar patterns to those of the south wall (see Fig. 9  $\sim$  Fig. 11). The roof absorbs the largest energy amounts compared to the other walls in the same building enclosure systems. The temperature can rise up to 57.3 °C and 42.4 °C for the dark and light systems, respectively, as shown in Fig. 9(c). However, the highest temperature can be reduced to 34.7 °C with the assistance of the SS-PCM. For the east wall, the peak temperature is 33.7 °C with the SS-PCM coating applied, which is increased by 44.2% and 5.6% once dark and light systems were implemented correspondingly, as seen in Fig. 10(a). The west wall shows similar results and patterns to those of the east wall, the main difference is that the peak temperature shifts from morning to afternoon, as

shown in Fig. 10(c). For the north wall, the temperature does not show great difference among the three systems since there is not a large amount of solar radiation reaching on the wall, although the SS-PCM still produces a significant cooling effect as shown in Fig. 11(a). To provide an overview of the results, the highest temperature and the total heat gains are summarized in Table 3.

On cold days, the temperature profiles of the SS-PCM coatings at different orientations of the building enclosure almost overlap with that of the dark system since the SS-PCM remains opaque most of the time, which is desirable, because the external temperature cannot trigger change phase in the coatings. Thus, the absorptivity of the SS-PCM (as shown in Fig. 6) and dark system (0.7) are almost identical, which lead to the performance of the SS-PCM and the black system is so similar in cold days. Fig. 12 shows, on the south wall and the roof, that there is a slight

 Table 3

 summary of the thermal results for different models.

| orientation | Material | summer                |                                  | winter                 |                      |  |
|-------------|----------|-----------------------|----------------------------------|------------------------|----------------------|--|
|             |          | $T_{peak}[^{\circ}C]$ | Heat gains [kWh/m <sup>2</sup> ] | T <sub>peak</sub> [°C] | Heat losses [kWh/m²] |  |
| South       | SS-PCM   | 34.5                  | 0.124                            | 24.3                   | 1.023                |  |
|             | dark     | 45.8(+32.7%)          | 0.296(+138.7%)                   | 26.8(+10.3%)           | 1.024(+0.01%)        |  |
|             | light    | 37.3(+8.1%)           | 0.164(+32.2%)                    | 11.7(-51.9%)           | 1.218(+0.19.1%)      |  |
| Roof        | SS-PCM   | 34.7                  | 0.154                            | 13.3                   | 1.216                |  |
|             | dark     | 57.3(+65.1%)          | 0.560(+263.6%)                   | 13.7(+3.0%)            | 1.206(-0.8%)         |  |
|             | light    | 42.4(+22.2%)          | 0.279(+81.2%)                    | 5.9(-55.6%)            | 1.302(+7.1%)         |  |
| East        | SS-PCM   | 33.7                  | 0.118                            | 11.5                   | 1.253                |  |
|             | dark     | 48.6(+44.2%)          | 0.356(+201.7%)                   | 11.6(+0.01%)           | 1.250(-0.2%)         |  |
|             | light    | 35.6(+5.6)            | 0.190(+61.0%)                    | 3.4(-70.4%)            | 1.321(+5.4%)         |  |
| west        | SS-PCM   | 34.2                  | 0.121                            | 15.2                   | 1.254                |  |
|             | dark     | 51.5(+50.6%)          | 0.366(+202.5%)                   | 15.2(0.0%)             | 1.251(-0.2%)         |  |
|             | light    | 39.5(+15.5%)          | 0.194(+60.3%)                    | 6.9(-54.6%)            | 1.321(+5.4%)         |  |
| north       | SS-PCM   | 31.7                  | 0.094                            | 2.9                    | 1.335                |  |
|             | dark     | 36.6(+15.5%)          | 0.209(+122.3%)                   | 2.9(0.0%)              | 1.335(0.0%)          |  |
|             | light    | 33.4(+5.4%)           | 0.129(+37.2%)                    | 1.5(-48.3%)            | 1.358(+1.7%)         |  |

Note: the numbers in the parenthesis mean the percentage respect to the corresponding value of SS-PCM.

difference on the temperature profiles of the SS-PCM system and the dark system, while the peak temperature on the light system is much less than that of the SS-PCM. In terms of the heat flux, the curves are below zero during most of the time in Fig. 12 (b) and (d), which means that most of the heat lost to its environment in winter, as expected. However, the heat flux of the SS-PCM system is closest to zero line and the heat loss is -1.023 kWh/m<sup>2</sup>, which is almost identical as that of the dark system and less than that of the light system. The heat flux is essentially zero during a short time period at noon with the SS-PCM system implemented on the south wall, which further illustrates the potential of the novel SS-PCM to achieve NZEBs. The same conclusion can be drawn on the east and west walls from Fig. 13, as the peak temperature and heat losses summarized in Table 3. Although the heat gains by the SS-PCM system cannot offset the heat losses in winter, it still captures more energy compared to the light system. Maximal energy saving can be achieved for building heating and cooling if there isn't any undesirable heat exchange (i.e., heat gain during summer and heat loss during winter) between indoor and outdoor environment through building enclosure.

The SS-PCM coatings, regardless of their orientation, demonstrate the intended working mechanisms of the system. Numerical simulation results indicate that the temperature of the back reflector in contact with the SS-PCM coating drops dramatically compared with both reference systems (which do not undergo a thermally-induced change in transparency) during the summer. The SS-PCM system behaves like an excellent solar reflector during summer with most of the solar energy being reflected back to the environment, resulting in a smaller cooling load compared to those of the dark and light systems. The results also illustrate that the implementation of the SS-PCM not only reduces the amount of energy during summer days but also takes advantage of solar radiation during the winter.

Simulation results of all different enclosure scenarios are summarized and can be compared in Table 3. A comparison of SS-PCM

coating performance with those of the dark and light systems, indicates that the SS-PCM system shows good overall cooling effect in summer and a heating effect in winter. Although the installation of the SS-PCM coatings does not result in a ZEB building, these systems exhibit the largest overall energy savings compared with the buildings featuring dark or light coating system. The performance of all coatings varies with its orientation as part of the building enclosure. Among the temperature reduction effects of the SS-PCM coatings on all building orientations, its implementation on the roof shows the maximum temperature reduction in summer by 22.6 °C compared to the dark system and by 7.7 °C compared to the light system. Heat gains of the roof also show the maximum reduction during the summer by 0.406 kWh/m<sup>2</sup> and 0.125 kWh/m<sup>2</sup> compared with the dark and light systems respectively. Therefore, the SS-PCM coating on the roof exhibits the best overall performance among the walls of all orientations. This can be attributed to the following two reasons (see Fig. 6 and Fig. 7 for the detail): First, the daytime in-coming angle  $\theta$  in hot days for the roof is the minimum compared to the walls of all orientations, which leads to a lowest absorptivity when using the SS-PCM coating/back reflector system; Second, the period during which the solar radiation reaches the roof surface is the longest, which means the effect of SS-PCM on reducing the undesirable heat gains lasts for the longest time when installed on the roof. Since the SS-PCM system on the roof can achieve the most overall energy saving based on one-day simulations, its performance over a year time period was further investigated.

#### 3.2. Year-long performance of SS-PCM systems installed on the roof

Fig. 14 shows the monthly average temperature of the back reflector among the building roofs with different materials: light, dark, and the SS-PCM, over one year time period. For the hot months (e.g., from May to September), the peak temperatures of the roof in July are around 51 °C and 37 °C for the dark and light

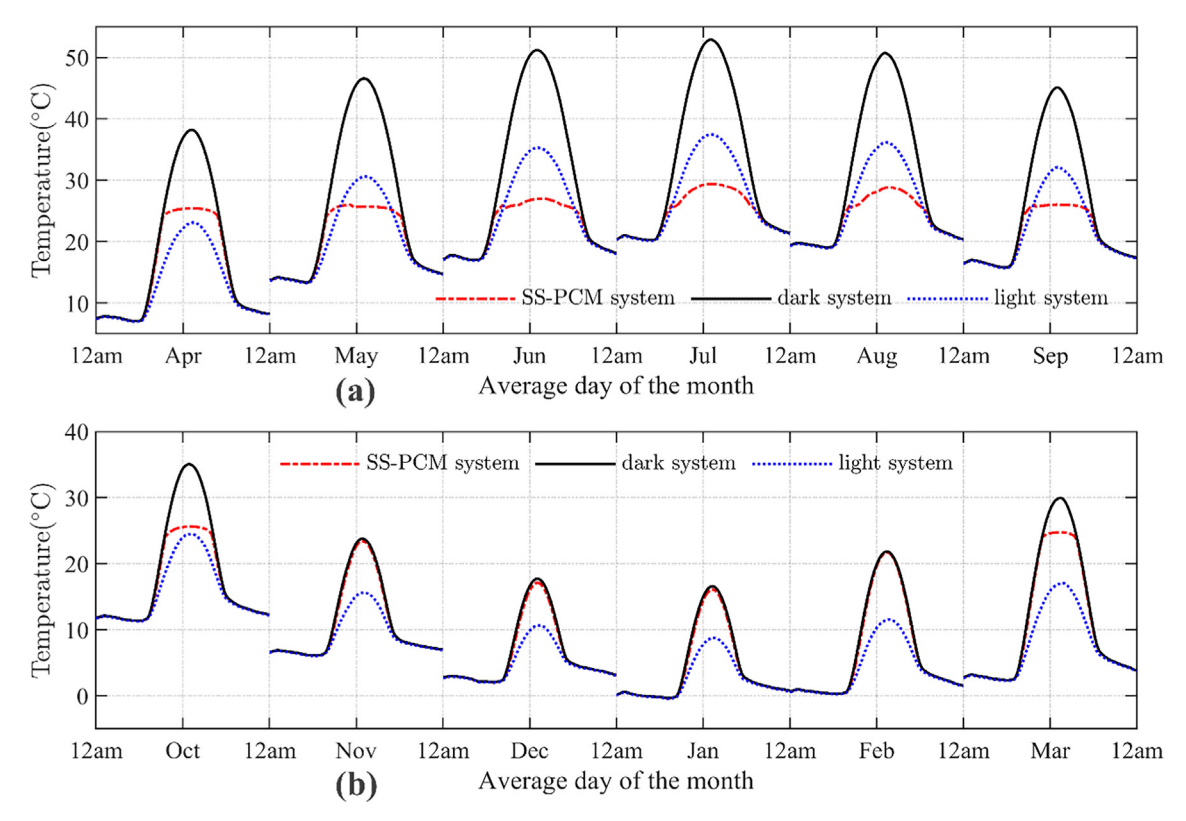


Fig. 14. Roof external surface temperature monthly averaged diurnal cycles of a year.

systems respectively, while that of the SS-PCM system is no more than 30 °C. For the cold months (e.g., from November to February), the temperature profiles of the SS-PCM system almost overlap with that of the dark system since the temperature is not high enough to trigger phase change. Fig. 15 shows the monthly average net heat flux into the room. In terms of the heat flux, the SS-PCM system remains very close to zero during daytime in some months like April or May, which verifies the potential of the SS-PCM to achieve ZEBs.

As expected, the light roof performs well in terms of heating absorption mitigation potential during the hot seasons of the year, where the roof is positively influenced by the relatively low radiative absorptivity for incoming solar irradiance. However, the SS-PCM behavior is even better in reducing the cooling load during the summer compared to that of the light system. Although cool roofs take advantage of solar radiation in summer, they inevitably suffer penalty during the winter months. The atypical temperature and heat flux profiles obtained for the SS-PCM roof are a consequence of its dynamic optical characteristics, which enables it to adjust its ability to absorb the incoming radiation as a function of the local surface temperature. Such an SS-PCM coated roof system is appealing to achieve NZEBs in cooling dominant climate zone, which has been very challenging for most of existing passive solar facades [2].

The use of the thermo-optically responsive SS-PCM coatings produces a more steady-state temperature profile from April to October, comparing to both the dark and the light configurations. This smooths the cooling energy demands, which is an additional positive effect of such an innovative application.

In order to compare the total annual energy consumption among three different roof systems, the total amount of energy flux flowing through the roof of the building was derived from the numerical simulation results. Energy loads were derived from the heat exchanged through a square meter of roof via heat flux inward

or outward to the exterior environment, Fig. 16 and Fig. 17 show the monthly cooling and heating loads for three types of roof systems throughout a year, respectively. To clearly show differences in the annual total cooling-heating load, Fig. 18 and Fig. 19 further illustrate the relative loads of the SS-PCM and light roofs compared with the dark roof system. Although the results indicate that the implementation of a light system reduces the amount of heat gains through the building during summer months, up to 5.234 kWh/m<sup>2</sup> in July compared with the dark roof, the light system always exhibits much larger heat losses during the colder months. The light system case, achieves more cooling savings, i.e., 26.050 kWh/m<sup>2</sup> compared with the dark system, but inevitably suffers from the higher heat losses throughout the year, increasing the heating loads by 14.283 kWh/m<sup>2</sup>. By using the SS-PCM coating, on one hand, the cooling energy load is dramatically reduced, up to 7.397 kWh/m<sup>2</sup>, compared to that of the dark system in July. Overall, as can be seen in Table 4, the SS-PCM coating reduces the annual cooling loads by 31.712 kWh/m<sup>2</sup>. On the other hand, the winter penalty of the low absorptivity of the light system is completely avoided in the colder months for the SS-PCM roof system. It performs as a solar energy absorber as well as the dark system which leads to a smaller energy loss during the winter. Overall, the SS-PCM system can save 29.60% and 18.26% of the total annual energy consumption compared to the dark and light system.

The dark system temperature profiles are always associated with the largest fluctuations, while the SS-PCM roof always presents surface temperature closest to the room temperature and heat flux nearest to zero during daytime.

## 3.3. Comparison among different phase transition temperatures

In this section, the results are presented to show the influence on the performance in building envelopes by the

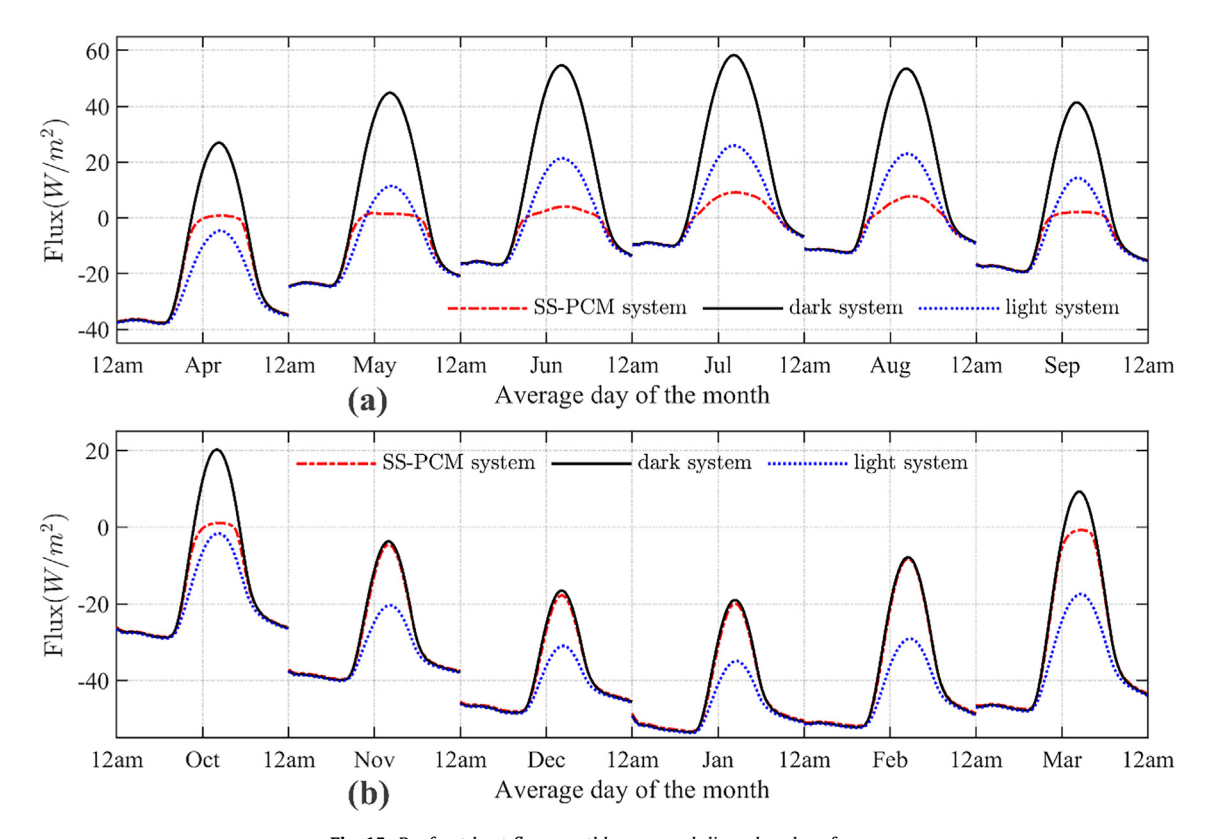


Fig. 15. Roof net heat flux monthly averaged diurnal cycles of a year.

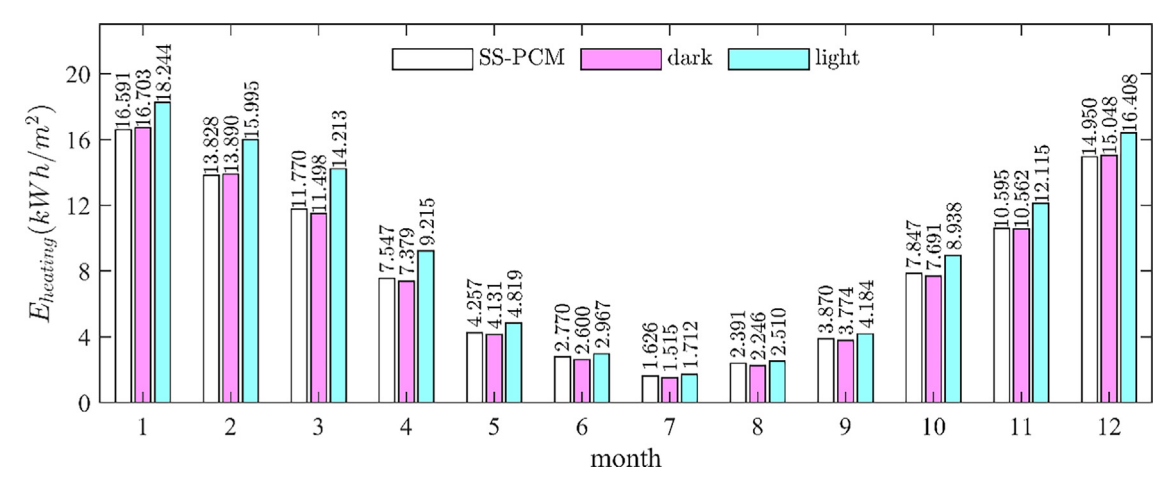
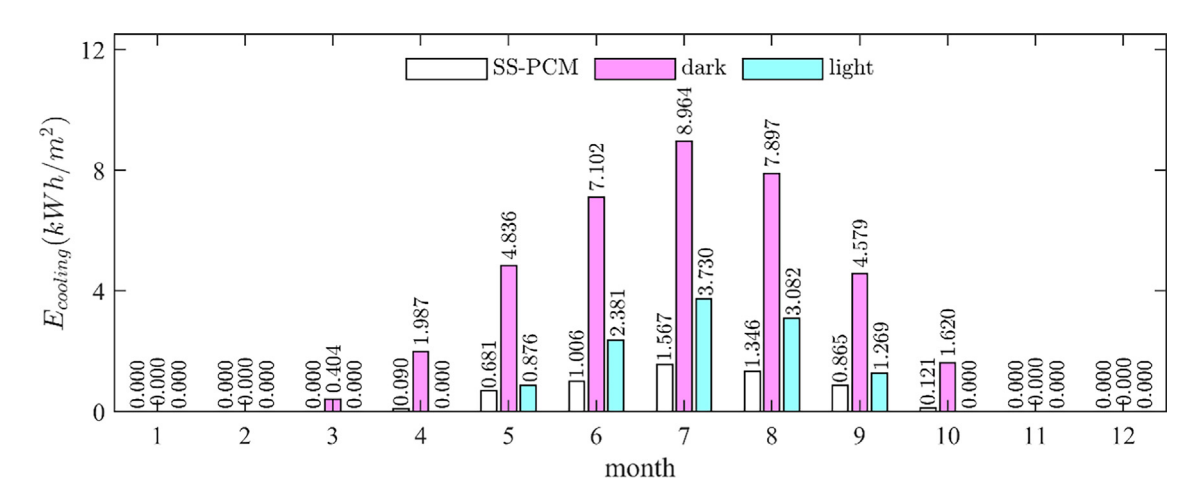


Fig. 16. Roof heating load monthly averaged values throughout a whole year.



 $\textbf{Fig. 17.} \ \ \textbf{Roof cooling load monthly averaged values throughout a whole year.}$ 

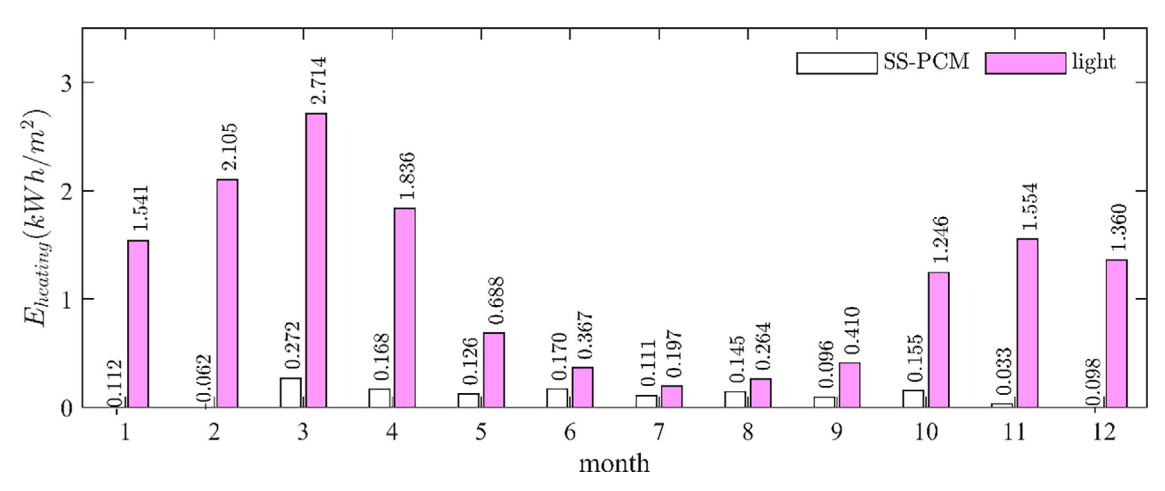


Fig. 18. Difference between heating load per meter square of the SS-PCM or light roof, relative to the dark roof, for each simulated month.

comparison of three SS-PCM materials with the same temperature-dependent transparency but different phase transition temperatures, i.e., TT=20, 25 and 30 °C. Each considered configuration is associated with the SS-PCM that is dynamically tuning its transparency in response to the applied temperature boundary condition.

Fig. 20 and Fig. 21 show cooling and heating loads for the SS-PCM roof systems with varying phase transition temperatures. These data show that the TT plays an important role on cooling loads: the SS-PCM roof system with higher TT leads to more cooling energy consumption than that of the SS-PCM with lower TT. For example, the cooling load value drops from 3.795 kWh/m²

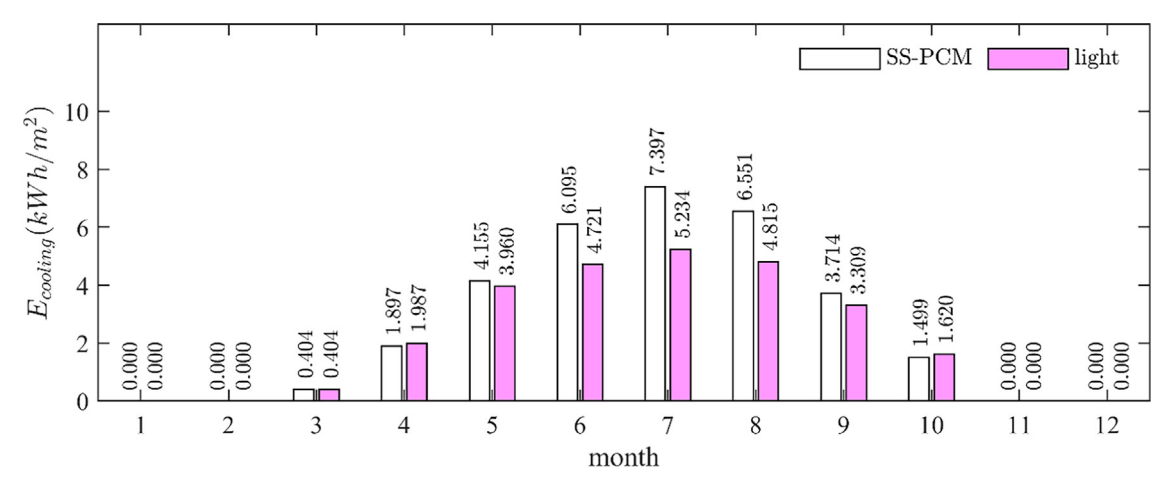
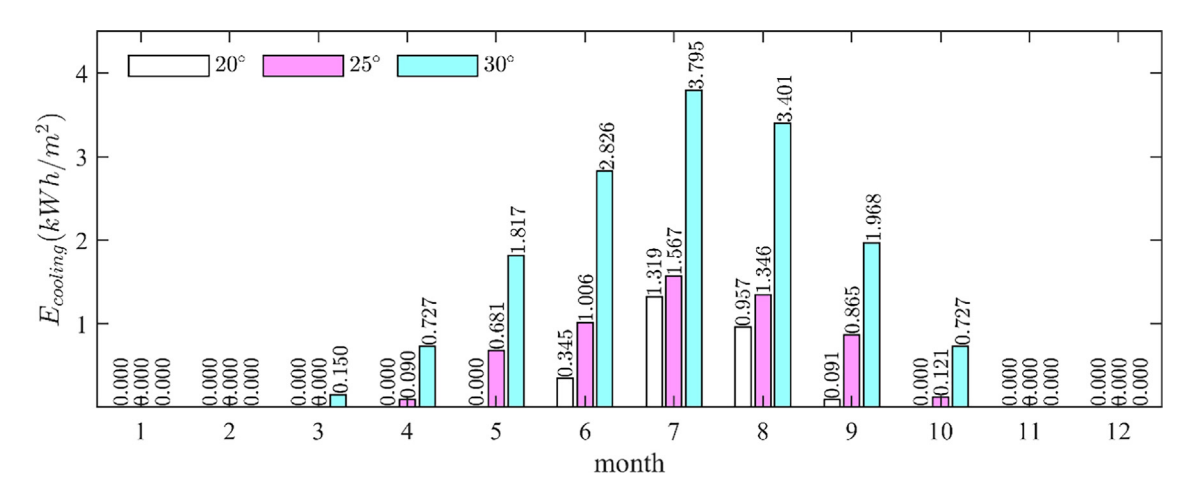


Fig. 19. Difference between cooling load per meter square of the SS-PCM or light roof, relative to the dark roof, for each simulated month.

**Table 4**Yearly cumulative energy loads per meter square of three types of roofs.

| material       | Cooling<br>[kWh/m²] | Cooling difference [kWh/m²]    | Heating<br>[kWh/m²] | Heating difference [kWh/m²]  | Summation [kWh/m²] | Summation difference [kWh/m²] |
|----------------|---------------------|--------------------------------|---------------------|------------------------------|--------------------|-------------------------------|
| SS-PCM<br>dark | 5.676<br>37.388     | 0 (0%)<br>31.712<br>(+558.70%) | 98.042<br>97.037    | 0 (0%)<br>-1.005<br>(-1.03%) | 103.718<br>134.425 | 0 (0%)<br>30.707<br>(+29.60%) |
| light          | 11.338              | 5.662<br>(+99.75%)             | 111.320             | 13.278<br>(+13.54%)          | 122.658            | 18.940<br>(+18.26%)           |

Note: the numbers in the parenthesis mean the difference respect to the corresponding value of SS-PCM.



 $\textbf{Fig. 20.} \ \ \text{Roof cooling loads monthly averaged values throughout a whole year for the three considered transition temperatures, i.e., 20, 25 \ \text{and } 30\ ^\circ\text{C}.$ 

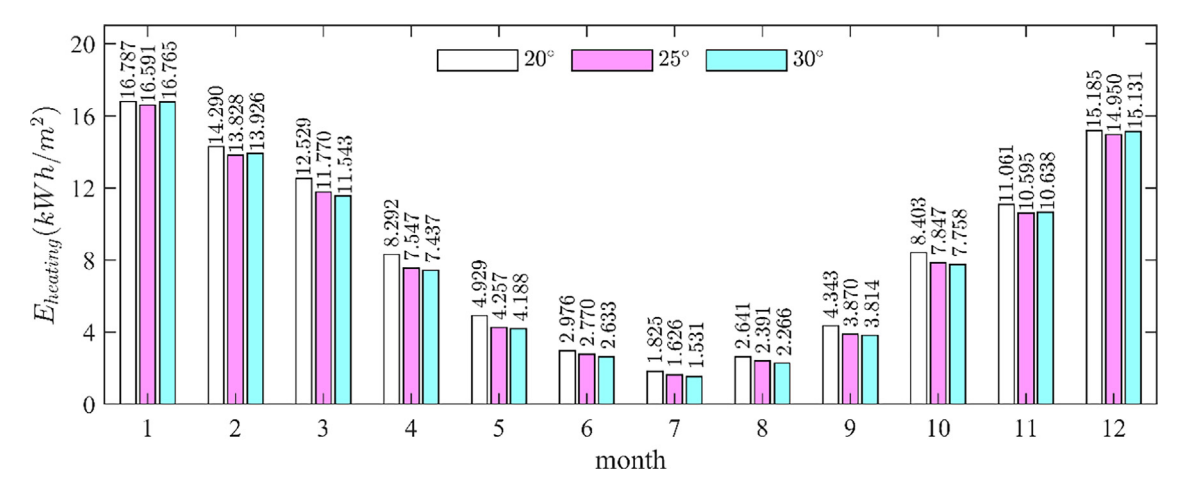


Fig. 21. Roof heating loads monthly averaged values throughout a whole year for the three considered transition temperatures, i.e., 20, 25 and 30 °C.

**Table 5**Yearly cumulative energy loads per meter square of three types of SS-PCM roofs.

| Phase change<br>temperature [°C] | cooling<br>[kWh/m²] | heating<br>[kWh/m²] | summation<br>[kWh/m²] |
|----------------------------------|---------------------|---------------------|-----------------------|
| TT = 20                          | 2.712               | 103.260             | 105.972               |
| TT = 25                          | 5.676               | 98.042              | 103.718               |
| TT = 30                          | 15.410              | 97.629              | 113.039               |

(TT = 30 °C) to 1.319 kWh/m² (TT = 20 °C) in the hottest month July. In terms of heating load, the SS-PCM roof system with lower TT results in higher heating energy consumption than that of the SS-PCM system with higher TT in transition seasons (e.g., February to November). For instance, the heating load rises from 11.543 kWh/m² (when TT = 30 °C) to 12.529 kWh/m² (when TT = 20 °C) in March. Table 5 summarizes the annual cumulative energy loads per meter square of three types of SS-PCM roofs. The SS-PCM roof system with TT equal to 25 °C consumes 103.718 kWh/m² per year which is smallest among the three SS-PCM roof systems.

Thus, the SS-PCM system with TT equal to  $25\,^{\circ}\mathrm{C}$  exhibits the best overall performance among the three cases, considering both the cooling and heating energy consumption over one year period. Due to the assumption that the room temperature was set at  $25\,^{\circ}\mathrm{C}$ , the minimum heat exchange between the indoor room and outside environment occurs when the transparency trigger was set as the same as the room temperature. In summary, it can be stated that, from an energy saving perspective, the most promising TT value of the SS-PCM roof system for the selected boundary conditions and roof insulation is  $25\,^{\circ}\mathrm{C}$ .

#### 3.4. Simulation under cooling-dominant climate

The numerical simulation results above demonstrate the advantages of the SS-PCM coating system under the climate of Boston, northeast of the United States, which is heating-dominant. To investigate the feasibility of using the SS-PCM building enclosure for energy saving or enabling nearly or net ZEBs in a cooling-dominant climate, the climate of Houston was chosen as the climatic conditions for a year-long simulation. All the other conditions of the simulation models remain the same as those of the Boston cases.

Fig. 22 shows the average temperature of the back reflector among the building envelopes with different roofs: light, dark, and the SS-PCM systems. With the SS-PCM roof system installed, the highest temperature does not surpass 35 °C throughout the vear, while the peak temperature can go beyond 60 °C and 45 °C for the dark and light systems, respectively. Fig. 23 shows the monthly average heat flux into the room. Throughout the year, the flux curve of SS-PCM system is always the closest to the zero-value line, which means least energy exchange between the interior room and the exterior environment. We can see the total accumulated heating and cooling loads in Table 6. Under the climate condition of Houston, the SS-PCM system can help obtain higher percentage of total energy saving, which is up to 79.7% compared with the corresponding value of 32.11% of Boston in Table 4. It also demonstrates the advantages of the SS-PCM in the warmer climate that has been a challenge for achieving ZEBs with most of existing passive solar façade systems [2]. Thus, the SS-PCM is promising not only in cold climate, like Boston, but also in warm climate like Houston. Remarkably, the SS-PCM coatings can

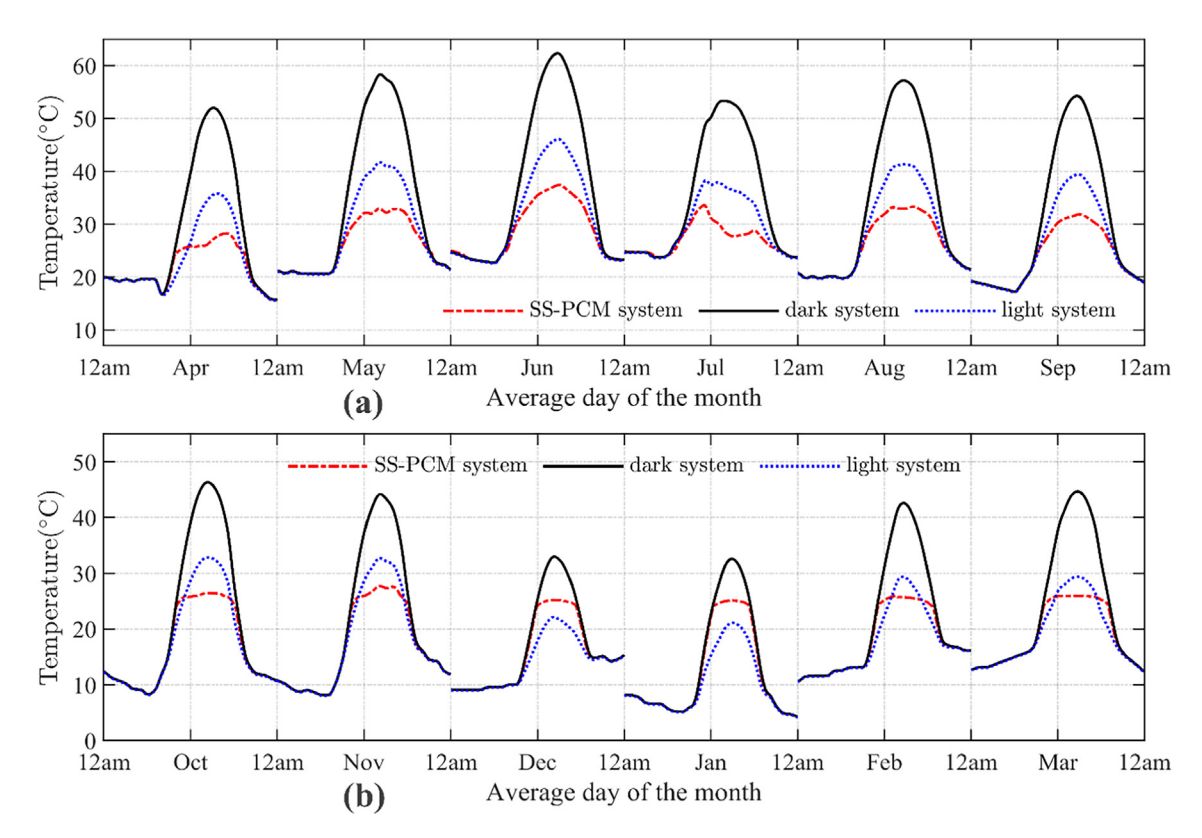


Fig. 22. Roof external surface temperature monthly averaged diurnal cycles of a year in Houston.

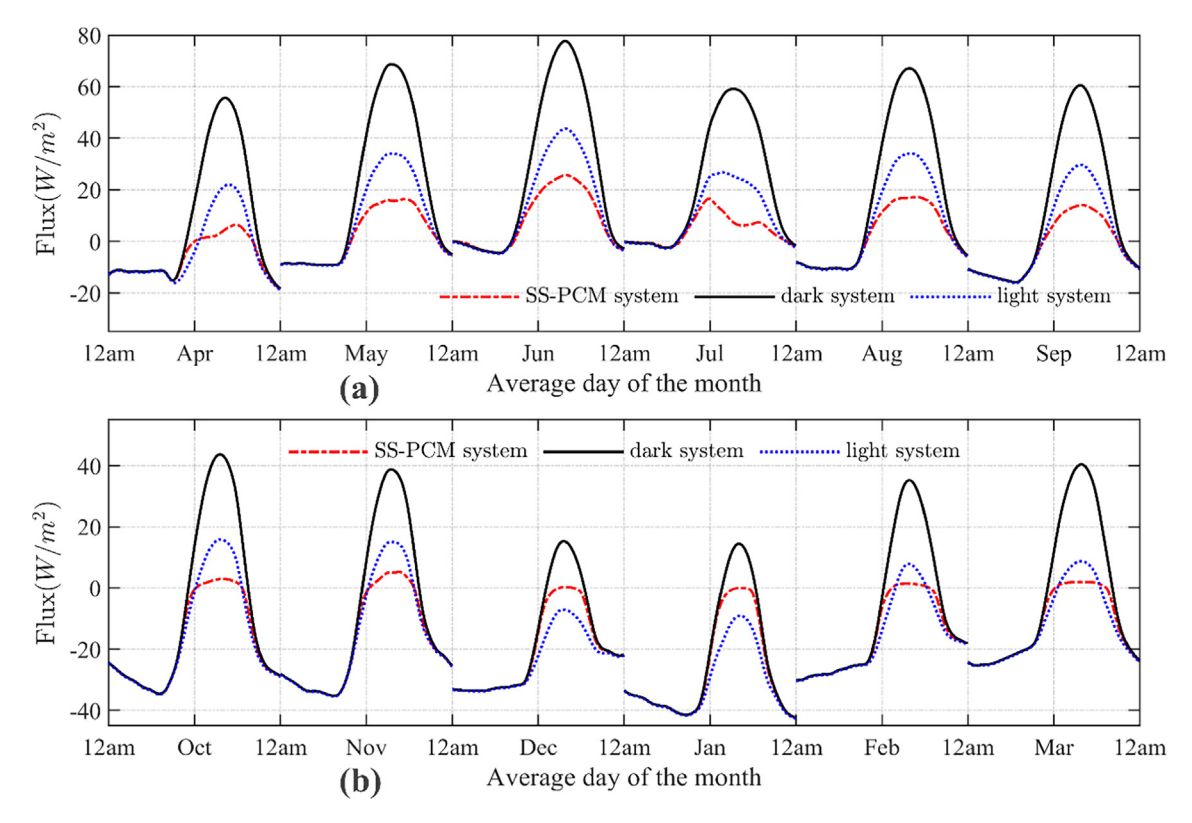


Fig. 23. Roof net heat flux monthly averaged diurnal cycles of a year in Houston.

**Table 6**Yearly cumulative energy loads per meter square of three types of roofs in Houston.

| material | Cooling<br>[kWh/m²] | cooling difference [kWh/m²] | Heating<br>[kWh/m²] | heating difference<br>[kWh/m²] | summation [kWh/m²] | summation difference [kWh/m²] |
|----------|---------------------|-----------------------------|---------------------|--------------------------------|--------------------|-------------------------------|
| SS-PCM   | 14.190              | 0<br>(0%)                   | 52.221              | 0<br>(0%)                      | 66.411             | 0<br>(0%)                     |
| dark     | 68.754              | 54.564<br>(+384.5%)         | 50.562              | -1.659<br>(-3.2%)              | 119.316            | 52.905<br>(+79.7%)            |
| light    | 28.951              | 14.761<br>(+104.0%)         | 56.866              | 4.645<br>(+8.9%)               | 85.817             | 19.406<br>(29.2%)             |

Note: the numbers in the parenthesis mean the difference respect to the corresponding value of SS-PCM.

achieve larger thermal benefits and higher potential to enable nearly or net ZEBs in the warmer climate.

#### 4. Conclusions

In this work, innovative, passive building enclosures with the thermo-optically responsive SS-PCM coating were proposed and evaluated to maximize energy saving through numerical simulations, by taking advantage of the synergies between the optical and thermal processes and its temperature-dependent transparency. The main findings are summarized below:

(1) The comparison of the simulations among dark, light and SS-PCM-coated systems shows that the SS-PCM system can reduce the heat gains in hot days while still taking advantage of solar heat in cold days. Simulation results confirm the potential of the SS-PCM system to eventually enable NZEBs and reduce undesirable heat exchange between the building enclosure in all orientations and its environment. In addition, the comparison of having the SS-PCM coating integrated at different orientations of a building enclosure shows that the performance of the SS-PCM system on the roof exhibits best overall thermal efficiency and maximal energy saving.

- (2) The comparison of year-long simulations among dark, light and SS-PCM-coated roofs demonstrates that the SS-PCM system is able to take advantage of solar energy throughout the year in saving under both heating and cooling loads relative to other systems. Notably, comparison of both the cooling and heating energy consumption among SS-PCM coatings with different phase transition temperatures, indicates that the optimal phase transition temperature should be set the same as the desirable room temperature.
- (3) Numerical simulation results confirm the feasibility of the SS-PCM system under heating-dominant and cooling-dominant climates, while the system shows larger thermal benefits and higher potential to achieve NZEBs in the warmer climate than in the colder climate zones. Although the results do not indicate that the building can be rendered a ZEB by installing the SS-PCM coatings, it shows the closest to ZEB performance compared to the buildings with installed dark or light system alone. The thermo-optically responsive SS-PCM coatings exhibit a greater potential to produce ZEBs, especially those in warm climate zones, which has been very challenging for most of existing passive solar facades [2].

In summary, using advanced building materials such as thermooptically responsive SS-PCMs in building enclosures can be a promising solution to achieve net or nearly ZEB since it can mitigate the increase of air temperatures in the urban environment during summer overheated conditions, while maintaining the positive absorption of solar radiation in winter. Future research should include whole-building modeling and experiments on building enclosure to verify potential energy benefits at the building level.

# **Declaration of Competing Interest**

The authors declare that they have no known competing financial interests or personal relationships that could have appeared to influence the work reported in this paper.

#### Acknowledgements

Support from the National Science Foundation, award numbers CMMI-1662903 & CMMI-1662675, Directorate for Engineering, Division of Civil, Mechanical and Manufacturing Innovation (CMMI), Structural and Architectural Engineering and Materials program (SAEM), is much appreciated.

#### References

- [1] E.I. Administration, EIA projects nearly 50% increase in world energy usage by 2050, in, 2019.
- [2] D. Ürge-Vorsatz, R. Khosla, R. Bernhardt, Y.C. Chan, D. Vérez, S. Hu, L.F. Cabeza, Advances toward a net-zero global building sector, Annu. Rev. Environ. Resour. 45 (2020) 227–269.
- [3] W. Wu, H.M. Skye, Net-zero nation: HVAC and PV systems for residential net-zero energy buildings across the United States, Energy Convers. Manage. 177 (2018) 605–628.
- [4] K. Sudhakar, M. Winderl, S.S. Priya, Net-zero building designs in hot and humid climates: a state-of-art, Case Stud. Therm. Eng. 13 (2019) 100400, https://doi. org/10.1016/j.csite.2019.100400.
- [5] M. Shin, J.-C. Baltazar, J.S. Haberl, E. Frazier, B. Lynn, Evaluation of the energy performance of a net zero energy building in a hot and humid climate, Energy Build. 204 (2019) 109531.
- [6] P. Penna, A. Prada, F. Cappelletti, A. Gasparella, Multi-objectives optimization of Energy Efficiency Measures in existing buildings, Energy Build. 95 (2015) 57–69
- [7] M.F. Hordeski, Dictionary of energy efficiency technologies, Dictionary of Energy Efficiency Technologies, (2004).
- [8] O. Saadatian, K. Sopian, C.H. Lim, N. Asim, M.Y. Sulaiman, Trombe walls: A review of opportunities and challenges in research and development, Renew. Sustain. Energy Rev. 16 (8) (2012) 6340–6351.
- [9] M.S. Sharma, N.D. Kaushika, Design and performance-characteristics of honeycomb solar pond, Energy Convers. Manage. 27 (1) (1987) 111–116.
- [10] N.D. Kaushika, K. Sumathy, Solar transparent insulation materials: a review, Renew. Sustain. Energy Rev. 7 (4) (2003) 317–351.
- [11] G.M. Wallner, R. Hausner, H. Hegedys, H. Schobermayr, R.W. Lang, Application demonstration and performance of a cellulose triacetate polymer film based transparent insulation wall heating system, Sol. Energy 80 (11) (2006) 1410– 1416.
- [12] J. Cadafalch, R. Cònsul, Detailed modelling of flat plate solar thermal collectors with honeycomb-like transparent insulation, Sol. Energy 107 (2014) 202–209.
- [13] E. Gratia, A. De Herde, Natural cooling strategies efficiency in an office building with a double-skin façade, Energy Build. 36 (11) (2004) 1139–1152.
- [14] M.A. Shameri, M.A. Alghoul, K. Sopian, M.F.M. Zain, O. Elayeb, Perspectives of double skin façade systems in buildings and energy saving, Renew. Sustain. Energy Rev. 15 (3) (2011) 1468–1475.
- [15] P. Bamfield, Chromic phenomena: technological applications of colour chemistry, Royal Society of Chemistry, 2010.
- [16] M. Aburas, V. Soebarto, T. Williamson, R. Liang, H. Ebendorff-Heidepriem, Y. Wu, Thermochromic smart window technologies for building application: a

- review, Appl. Energy 255 (2019) 113522, https://doi.org/10.1016/j.apenergy.2019.113522.
- [17] P.S. Aklujkar, B. Kandasubramanian, A review of microencapsulated thermochromic coatings for sustainable building applications, J. Coat. Technol. Res. 18 (1) (2021) 19–37.
- [18] Y. Cui, Y. Ke, C. Liu, Z. Chen, N. Wang, L. Zhang, Y. Zhou, S. Wang, Y. Gao, Y.i. Long, Thermochromic VO2 for energy-efficient smart windows, Joule 2 (9) (2018) 1707–1746.
- [19] M. Casini, Active dynamic windows for buildings: a review, Renewable Energy 119 (2018) 923–934.
- [20] Z. Zhang, Y. Gao, Z. Chen, J. Du, C. Cao, L. Kang, H. Luo, Thermochromic VO2 thin films: solution-based processing, improved optical properties, and lowered phase transformation temperature, Langmuir 26 (13) (2010) 10738–10744.
- [21] L. Long, H. Ye, 10 Nano-based chromogenic technologies for building energy efficiency, in: F. Pacheco-Torgal, E. Rasmussen, C.-.-G. Granqvist, V. Ivanov, A. Kaklauskas, S. Makonin (Eds.), Start-Up Creation, Woodhead Publishing, 2016, pp. 213–236.
- [22] C.G. Granqvist, Y.-X. Ji, J. Montero, G.A. Niklasson, Thermochromic vanadium-dioxide-based thin films and nanoparticles: Survey of some buildings-related advances, J. Phys. Conf. Ser 764 (2016) 012002, https://doi.org/10.1088/1742-6596/764/1/012002.
- [23] J. Kośny, PCM-Enhanced Building Components: An Application of Phase Change Materials in Building Envelopes and Internal Structures, Springer, 2015
- [24] A. Sharma, V.V. Tyagi, C.R. Chen, D. Buddhi, Review on thermal energy storage with phase change materials and applications, Renew. Sustain. Energy Rev. 13 (2) (2009) 318–345.
- [25] M.M. Farid, A.M. Khudhair, S.A.K. Razack, S. Al-Hallaj, A review on phase change energy storage: materials and applications, Energy Convers. Manage. 45 (9) (2004) 1597–1615.
- [26] M. Esen, Thermal performance of a solar-aided latent heat store used for space heating by heat pump, Sol. Energy 69 (1) (2000) 15–25.
- [27] M. Esen, T. Ayhan, Development of a model compatible with solar assisted cylindrical energy storage tank and variation of stored energy with time for different phase change materials, Energy Convers. Manage. 37 (12) (1996) 1775–1785
- [28] C.J.P.A.M.-A.S.I.S.E.S. Swet, Phase change storage in passive solar architecture, 5 (CONF-801016-(Vol. 1)) (1980).
- [29] L.F. Cabeza, A. Castell, C. Barreneche, A. de Gracia, A.I. Fernández, Materials used as PCM in thermal energy storage in buildings: a review, Renew. Sustain. Energy Rev. 15 (3) (2011) 1675–1695.
- [30] L.A. Chidambaram, A.S. Ramana, G. Kamaraj, R. Velraj, Review of solar cooling methods and thermal storage options, Renew. Sustain. Energy Rev. 15 (6) (2011) 3220–3228.
- [31] A. Fallahi, G. Guldentops, M. Tao, S. Granados-Focil, S. Van Dessel, Review on solid-solid phase change materials for thermal energy storage: Molecular structure and thermal properties, Appl. Therm. Eng. 127 (2017) 1427–1441.
- [32] G. Guldentops, G. Ardito, M. Tao, S. Granados-Focil, S. Van Dessel, A numerical study of adaptive building enclosure systems using solid-solid phase change materials with variable transparency, Energy Build. 167 (2018) 240–252.
- [33] P. Mishra, K. Stockmal, G. Ardito, M. Tao, S. Van Dessel, S. Granados-Focil, Thermo-optically responsive phase change materials for passive temperature regulation, Sol. Energy 197 (2020) 222–228.
- [34] T.L. Bergman, F.P. Incropera, D.P. DeWitt, A.S. Lavine, Fundamentals of Heat and Mass Transfer, John Wiley & Sons, 2011.
- [35] ASHRAE HANDBOOK-FUNDAMENTALS, SI Edition ed., ASHRAE, 2013.
- [36] A. Roy, R. Ramasubramaniam, H.A.J.J.o.b.o. Gaonkar, Empirical relationship between Kubelka-Munk and radiative transfer coefficients for extracting optical parameters of tissues in diffusive and nondiffusive regimes, 17(11) (2012) 115006.
- [37] G.B. Cordon, M.G.J.J.o.c.e. Lagorio, Absorption and scattering coefficients: a biophysical-chemistry experiment using reflectance spectroscopy, 84(7) 2007 1167.
- [38] M.G. Emmel, M.O. Abadie, N. Mendes, New external convective heat transfer coefficient correlations for isolated low-rise buildings, Energy Build. 39 (3) (2007) 335–342.
- [39] T. Min, L. Schutrum, G. Parmelee, J.J.A.T. Vouris, Natural convection and radiation in a panel heated room, 62 (1) (1956) 337-358.
- [40] EnergyPlus weather data in, EnergyPlus.